

Mixed-Dimensional Auxiliary Space Preconditioners

Ana Budiša*, Wietse M. Boon†, Xiaozhe Hu‡

Abstract

This work introduces nodal auxiliary space preconditioners for discretizations of mixed-dimensional partial differential equations. We first consider the continuous setting and generalize the regular decomposition to this setting. With the use of conforming mixed finite element spaces, we then expand these results to the discrete case and obtain a decomposition in terms of nodal Lagrange elements. In turn, nodal preconditioners are proposed analogous to the auxiliary space preconditioners of Hiptmair and Xu [16]. Numerical experiments show the performance of this preconditioner in the context of flow in fractured porous media.

1 Introduction

In recent work [7, 8, 25], exterior calculus and its finite element discretization has been extended to the mixed-dimensional geometries. More precisely, for an n -dimensional domain, sub-manifolds of dimension $n-1$ and their intersections of dimension $n-2$, $n-3$, and so on are considered. Suitable spaces of alternating k -forms are introduced and equipped with proper inner products and norms. Based on well-defined differential operators and codifferential operators, a de Rham complex for the mixed-dimensional geometry is proposed as well. Such a generalization of fixed-dimensional finite element exterior calculus [4] provides a unified theoretical framework for mixed-dimensional partial differential equations (PDEs) as well as their finite element discretizations. This has wide applications in mathematical modeling and simulation, e.g., shells, membranes, fractures, and geological formations [5, 10, 26].

One important result in the fixed-dimensional finite element exterior calculus is the stable regular decomposition and its discrete variant [14, 16]. Understanding the stable regular decompositions is at the heart of designing robust preconditioners for solving $H(\nabla \times)$ - and $H(\nabla \cdot)$ -elliptic problems based on the auxiliary space preconditioning framework [24, 29]. Based on the discrete regular decomposition, preconditioners for $H(\nabla \times)$ - and $H(\nabla \cdot)$ -elliptic problems can be developed, which consists of solving several $H(\nabla)$ -elliptic problems and simple smoothing steps in the original space. Numerical results [19, 20] have shown the effectiveness of such preconditioners.

In this work, we extend the stable regular decomposition to the mixed-dimensional geometries. Unlike the fixed-dimensional case, where the stable regular decomposition is usually derived based on the corresponding regular inverse, in the mixed-dimensional setting, we construct the regular decomposition directly by establishing such a regular decomposition on each individual sub-manifold and then combining them together properly. Discrete regular decomposition is also generalized to the mixed-dimensional geometries. The construction of the discrete version is similar with the fixed-dimensional counterpart. The resulting discrete regular decomposition also involves an extra high-frequency term comparing with the stable regular decomposition as expected. Based on discrete regular decomposition and auxiliary space preconditioning framework, we are able to develop robust preconditioners for solving abstract model mixed-dimensional PDEs (5.1).

In order to demonstrate the effectiveness of the proposed auxiliary space preconditioner for solving mixed-dimensional PDEs, we consider flow in fractured porous media as an example, which is modeled by Darcy's law and conservation of mass in the mixed-dimensional setting. After discretization, robust block preconditioners are designed based on the well-posedness of the discrete

¹Department of Mathematics, University of Bergen, Allegaten 41, P. O. Box 7803, N-5020 Bergen, Norway. Ana.Budisa@uib.no

²Department of Mathematics, KTH Royal Institute of Technology, Lindstedtsvägen 25, 10044 Stockholm, Sweden.

³Department of Mathematics, Tufts University, 503 Boston Ave, Medford, MA 02155, USA.

PDEs based on the framework developed in [22,23]. The mixed-dimensional auxiliary space preconditioner is used to invert one of the diagonal blocks in the block preconditioners. The effectiveness of the preconditioners are verified both theoretically and numerically.

The rest of the paper is organized as follows. Section 2 introduces the mixed-dimensional geometries and function spaces. Mixed-dimensional regular decomposition is derived in Section 3 and the discrete version is proposed in Section 4. In Section 5, we describe the mixed-dimensional auxiliary space preconditioner for abstract mixed-dimensional PDEs and an example, flow in fractured porous media, is introduced in Section 6. Numerical results are shown in Section 7 to demonstrate the robustness and effectiveness of the proposed preconditioners, and the conclusions are given in Section 8.

2 Preliminaries

In this section, we first introduce the definition of a mixed-dimensional geometry and the conventions used when referring to certain structures. Next, we summarize the relevant concepts from functional analysis for the fixed-dimensional case as well as the generalization to the mixed-dimensional setting. For a more rigorous and detailed exposition of these results, we refer the readers to [7].

2.1 Geometry

Given a contractible Lipschitz domain $Y \subset \mathbb{R}^n$ with $n \leq 3$. Within Y , we introduce disjoint manifolds $\Omega_i^{d_i}$ with i being the index from a global set I and d_i being the dimension. The superscript generally is omitted. Let I^d be the subset of I containing all indices i with $d_i = d$.

We refer to the union of all manifolds Ω_i as the mixed-dimensional geometry Ω and denote the subset of d -manifolds as Ω^d , i.e.

$$\Omega := \bigcup_{i \in I} \Omega_i, \quad \Omega^d := \bigcup_{i \in I^d} \Omega_i.$$

For each Ω_i with $i \in I$, we form a connection to each lower-dimensional manifold that coincides with (a portion of) its boundary. Each of these connections is endowed with a unique index j . Then, let i_j be the index of the lower-dimensional manifold such that $\Omega_{i_j} \subseteq \partial\Omega_i$. We denote $\partial_j\Omega_i$ as the corresponding boundary of dimension $d_j := d_{i_j}$.

For each $i \in I$ and $d < d_i$, we define I_i^d as the set of indices j such that $\partial_j\Omega_i$ is d -dimensional. Moreover, let I_i contain all indices j for which $\partial_j\Omega_i$ is not empty:

$$I_i^d := \{j : \exists i_j \in I^d \text{ such that } \partial\Omega_i \cap \Omega_{i_j} \neq \emptyset\}, \quad I_i := \bigcup_{d=0}^{d_i-1} I_i^d.$$

To exemplify a mixed-dimensional geometry Ω , let us consider Figure 1 and its corresponding index sets I_i^d . In this case, we have $I_2^d = \{12, 13\}$ with $i_{12} = 5$ and $i_{13} = 3$ and $I_2^0 = 16$ with $i_{16} = 6$. We note that two distinct portions of the boundary $\partial\Omega_1$ coincide geometrically with Ω_4 . This is represented by the two indices $\{9, 10\} \subset I_1^1$ with $i_9 = i_{10} = 4$.

2.2 Function Spaces

The next step is to define a function \mathbf{a} on the mixed-dimensional geometry. We do this using the language of exterior calculus [27]. We first introduce local function spaces on each subdomain which form the building blocks for the mixed-dimensional generalization.

For $i \in I$, let $\Lambda^k(\Omega_i)$ denote the space of differential k -forms on Ω_i . Let $L^2\Lambda^k(\Omega_i)$ denote the space of square integrable k -forms and $H\Lambda^k(\Omega_i)$ denote its subspace of forms with square integrable differential. In other words, let

$$L^2\Lambda^k(\Omega_i) := \{a_i \in \Lambda^k(\Omega_i) : \|a_i\|_{L^2(\Omega_i)} < \infty\}, \\ H\Lambda^k(\Omega_i) := \{a_i \in L^2\Lambda^k(\Omega_i) : da_i \in L^2\Lambda^{k+1}(\Omega_i)\}.$$

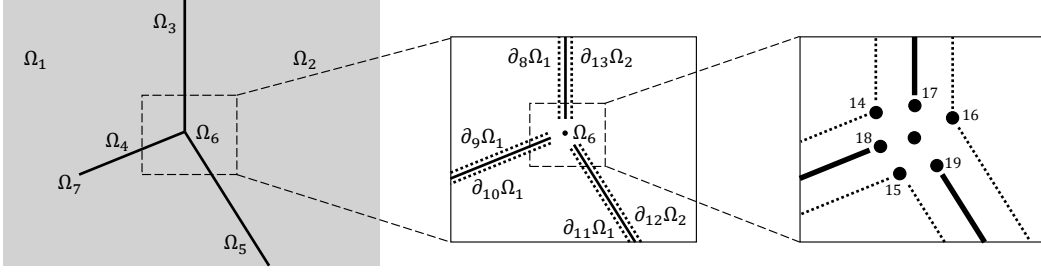


Figure 1: Example of a mixed-dimensional geometry with $n = 2$. On the left, Ω_i labels each d_i -manifold with $i \in I$. The index sets I^d for this geometry are as follows. $I^2 = \{1, 2\}$ represents the 2-manifolds, $I^1 = \{3, 4, 5\}$ denotes the 1-manifolds and the 0-manifolds in this geometry have indices $i \in I^0 = \{6, 7\}$. The middle of the figure illustrates the enumeration of boundaries $\partial_j \Omega_i$ for $i \in I^2$ and $j \in I_i^1$. On the right, the indices j are shown with the property $i_j = 6$.

With the exterior derivative d , the spaces $H\Lambda^k$ form a cochain complex, known as the de Rham complex:

$$H\Lambda^0(\Omega_i) \xrightarrow{d} H\Lambda^1(\Omega_i) \xrightarrow{d} \dots \xrightarrow{d} H\Lambda^{d_i-1}(\Omega_i) \xrightarrow{d} H\Lambda^{d_i}(\Omega_i).$$

We often use the correspondence of this complex to conventional Sobolev spaces. For $d_i = 3$, this representation of the de Rham complex is given by

$$H(\nabla, \Omega_i) \xrightarrow{\nabla} H(\nabla \times, \Omega_i) \xrightarrow{\nabla \times} H(\nabla \cdot, \Omega_i) \xrightarrow{\nabla \cdot} L^2(\Omega_i). \quad (2.1)$$

Here, $L^2(\Omega_i)$ is the space of square-integrable functions on Ω_i and the space $H(\nabla, \Omega_i)$ is its subspace of functions with square-integrable gradients, typically denoted by $H^1(\Omega_i)$. The spaces $H(\nabla \times, \Omega_i)$ and $H(\nabla \cdot, \Omega_i)$ are defined analogously.

We use the local spaces $L^2\Lambda^k$ and $H\Lambda^k$ to introduce the Sobolev spaces containing mixed-dimensional differential k -forms on Ω . For brevity, we omit the reference to the geometry and define

$$\begin{aligned} L^2\mathfrak{L}^k &:= \prod_{i \in I} \{a_i \in L^2\Lambda^{k_i}(\Omega_i) : \text{Tr}_j a_i \in L^2\Lambda^{k_i}(\Omega_{i_j}), \forall j \in I_i\}, \\ H\mathfrak{L}^k &:= \prod_{i \in I} \{a_i \in H\Lambda^{k_i}(\Omega_i) : \text{Tr}_j a_i \in H\Lambda^{k_i}(\Omega_{i_j}), \forall j \in I_i\}, \end{aligned}$$

with $k_i := d_i - (n - k)$. Here, and in the following, we interpret $\Lambda^k(\Omega_i)$ as zero for $k < 0$ and $k > d_i$. Thus, we emphasize that $H\mathfrak{L}^k$ is zero on manifolds Ω_i with $d_i < n - k$. The operator Tr_j is a trace operator that restricts a form a_i to $\partial_j \Omega_i$. We emphasize that for a given $\mathbf{a} = (a_i)_{i \in I} \in H\mathfrak{L}^k$, the component a_i has a well-defined trace on each $\partial_j \Omega_i$ for $j \in I_i$ with $k_i \leq d_j < d_i$ by definition.

The Gothic font is used to denote a mixed-dimensional differential form $\mathbf{a} \in H\mathfrak{L}^k$ and we revert to classic fonts with a subscript i to denote its component defined on Ω_i . In the analysis, we often use the corresponding restriction operator ι_i defined such that

$$\iota_i \mathbf{a} = a_i.$$

Next, we define the jump operator $\mathfrak{d} : H\mathfrak{L}^k \mapsto H\mathfrak{L}^{k+1}$. For each $i \in I$, let

$$\iota_i \mathfrak{d} \mathbf{a} = (-1)^{n-k} \sum_{l \in I^{d_i+1}} \sum_{\{j \in I_l : i_j = i\}} \text{Tr}_j a_l.$$

For more details on the definition of \mathfrak{d} , we refer to [7]. The mixed-dimensional differential \mathfrak{d} is formed as the sum of \mathfrak{d} and the exterior derivative d such that

$$\iota_i \mathfrak{d} \mathbf{a} = da_i + \iota_i \mathfrak{d} \mathbf{a}, \quad i \in I.$$

We introduce the following norms for $\mathbf{a} \in H\mathfrak{L}^k$:

$$\begin{aligned}\|\mathbf{a}\|_{L^2\mathfrak{L}^k}^2 &:= \sum_{i \in I} \|a_i\|_{L^2(\Omega_i)}^2 + \sum_{d=k_i}^{d_i} \sum_{j \in I_i^d} \|\text{Tr}_j a_i\|_{L^2(\Omega_{i_j})}^2, \\ \|\mathbf{a}\|_{H\mathfrak{L}^k}^2 &:= \|\mathbf{a}\|_{L^2\mathfrak{L}^k}^2 + \|\mathfrak{d}\mathbf{a}\|_{L^2\mathfrak{L}^{k+1}}^2.\end{aligned}$$

The inner products that naturally induce these norms are denoted by $(\cdot, \cdot)_{L^2\mathfrak{L}^k}$ and $(\cdot, \cdot)_{H\mathfrak{L}^k}$, respectively. The spaces $H\mathfrak{L}^k$ form a cochain complex which we refer to as the mixed-dimensional de Rham complex:

$$H\mathfrak{L}^0 \xrightarrow{\mathfrak{d}} H\mathfrak{L}^1 \xrightarrow{\mathfrak{d}} \dots \xrightarrow{\mathfrak{d}} H\mathfrak{L}^{n-1} \xrightarrow{\mathfrak{d}} H\mathfrak{L}^n. \quad (2.2)$$

This complex has several key properties, which we present in the following Lemma.

Lemma 2.1. *The complex (2.2) satisfies the following:*

- All exact forms are closed: each $\mathbf{a} \in H\mathfrak{L}^k$ satisfies

$$\mathfrak{d}(\mathfrak{d}\mathbf{a}) = 0. \quad (2.3)$$

- All closed forms are exact: for each $\mathbf{a} \in H\mathfrak{L}^k$ with $\mathfrak{d}\mathbf{a} = 0$, there exists a $\mathbf{b} \in H\mathfrak{L}^{k-1}$ such that

$$\mathfrak{d}\mathbf{b} = \mathbf{a}, \quad \|\mathbf{b}\|_{H\mathfrak{L}^{k-1}} \lesssim \|\mathbf{a}\|_{H\mathfrak{L}^k} \quad (2.4)$$

Proof. The proof can be found in [7]. \square

We represent this complex in terms of local spaces for each dimension. For $n = 3$, these local spaces are then organized in the following diagram:

$$\begin{array}{ccccccc} H\mathfrak{L}^0 & & H(\nabla, \text{Tr}; \Omega^3) & & & & \\ \downarrow \mathfrak{d} & & \downarrow \nabla & \searrow \mathfrak{d} & & & \\ H\mathfrak{L}^1 & & H(\nabla \times, \text{Tr}; \Omega^3) & & H(\nabla^\perp, \text{Tr}; \Omega^2) & & \\ \downarrow \mathfrak{d} & & \downarrow \nabla \times & \searrow \mathfrak{d} & \downarrow \nabla^\perp & \searrow \mathfrak{d} & \\ H\mathfrak{L}^2 & & H(\nabla \cdot, \text{Tr}; \Omega^3) & & H(\nabla \cdot, \text{Tr}; \Omega^2) & & H(\nabla \cdot, \text{Tr}; \Omega^1) \\ \downarrow \mathfrak{d} & & \downarrow \nabla \cdot & \searrow \mathfrak{d} & \downarrow \nabla \cdot & \searrow \mathfrak{d} & \downarrow \nabla \cdot & \searrow \mathfrak{d} \\ H\mathfrak{L}^3 & & L^2(\Omega^3) & & L^2(\Omega^2) & & L^2(\Omega^1) & & L^2(\Omega^0) \end{array} \quad (2.5)$$

Here, $\nabla \cdot$ denotes the divergence tangential to each manifold Ω_i , regardless of dimension. The curl is denoted by $\nabla \times$ in three dimensions and is given by the rotated gradient ∇^\perp on two-dimensional manifolds. The operator ∇ at the top of the diagram represents the gradient on three-dimensional subdomains.

The local function spaces are given by subspaces of conventional Sobolev spaces with extra trace regularity. By defining ν as the outward, unit normal vector on $\partial\Omega_i$ for $i \in I$, we define

$$\begin{aligned} H(\nabla \cdot, \text{Tr}; \Omega_i) &:= \{a_i \in H(\nabla \cdot, \Omega_i) : (\nu \cdot a_i)|_{\partial_j \Omega_i} \in L^2(\Omega_{i_j}), \quad \forall j \in I_i^{d_i-1}\}, \\ H(\nabla \times, \text{Tr}; \Omega_i) &:= \{a_i \in H(\nabla \times, \Omega_i) : (-\nu \times a_i)|_{\partial_j \Omega_i} \in H(\nabla \cdot, \text{Tr}; \Omega_{i_j}), \quad \forall j \in I_i^{d_i-1}\}, \\ H(\nabla^\perp, \text{Tr}; \Omega_i) &:= \{a_i \in H(\nabla^\perp, \Omega_i) : (\nu^\perp a_i)|_{\partial_j \Omega_i} \in H(\nabla \cdot, \text{Tr}; \Omega_{i_j}), \quad \forall j \in I_i^{d_i-1}\}, \\ H(\nabla, \text{Tr}; \Omega_i) &:= \{a_i \in H(\nabla, \Omega_i) : (a_i)|_{\partial_j \Omega_i} \in H(\nabla \times, \text{Tr}; \Omega_{i_j}), \quad \forall j \in I_i^{d_i-1}\}. \end{aligned}$$

The spaces in diagram (2.5) are then defined as the product of these spaces over all $i \in I^d$ for a given dimension d .

3 Regular Decomposition

The aim of this section is to show that the conventional regular decomposition of differential k -forms can be generalized to the mixed-dimensional setting. For that purpose, we first recall the fixed-dimensional regular decomposition in the continuous case. Then, we introduce the subspace of $H\Lambda^k$, that contains functions with higher regularity, and the analogous subspace of $H\mathfrak{L}^k$. In turn, this gives the main ingredients in the derivation of the mixed-dimensional regular decomposition.

3.1 Fixed-dimensional Regular Decomposition

We start with presenting the regular decomposition in the context of the de Rham complex (2.1). Given Ω_i with $d_i = 3$, we follow the results in [16] and provide the regular decomposition of $H(\nabla \cdot, \Omega_i)$ and $H(\nabla \times, \Omega_i)$ in the following theorems.

Theorem 3.1 (Regular decomposition of $H(\nabla \times, \Omega_i)$). *For any $\mathbf{q} \in H(\nabla \times, \Omega_i)$, there exist functions $\mathbf{a} \in (H(\nabla, \Omega_i))^3$ and $c \in H(\nabla, \Omega_i)$ such that*

$$\mathbf{q} = \mathbf{a} + \nabla c, \quad (3.1a)$$

$$\|\mathbf{a}\|_{H(\nabla, \Omega_i)} + \|c\|_{H(\nabla, \Omega_i)} \lesssim \|\mathbf{q}\|_{H(\nabla \times, \Omega_i)}. \quad (3.1b)$$

Theorem 3.2 (Regular decomposition of $H(\nabla \cdot, \Omega_i)$). *For any $\mathbf{q} \in H(\nabla \cdot, \Omega_i)$, there exist functions $\mathbf{a}, c \in (H(\nabla, \Omega_i))^3$ such that*

$$\mathbf{q} = \mathbf{a} + \nabla \times c, \quad (3.2a)$$

$$\|\mathbf{a}\|_{H(\nabla, \Omega_i)} + \|c\|_{H(\nabla, \Omega_i)} \lesssim \|\mathbf{q}\|_{H(\nabla \cdot, \Omega_i)}. \quad (3.2b)$$

Now, let $H_0(\nabla \times, \Omega_i)$ and $H_0(\nabla \cdot, \Omega_i)$ be the subspaces of $H(\nabla \cdot, \Omega_i)$ and $H(\nabla \times, \Omega_i)$, respectively, with zero trace on the boundary $\partial\Omega_i$. Also, denote the vector function space $\mathbf{H}_0(\nabla, \Omega_i) = \{\mathbf{u} \in (H(\nabla, \Omega_i))^3, \mathbf{u}|_{\partial\Omega_i} = \mathbf{0}\}$. The "boundary aware" regular decompositions from [15] are given in the following theorems.

Theorem 3.3 (Regular decomposition of $H_0(\nabla \times, \Omega_i)$). *For any $\mathbf{q} \in H_0(\nabla \times, \Omega_i)$, there exist functions $\mathbf{a} \in \mathbf{H}_0(\nabla, \Omega_i)$ and $c \in H_0(\nabla, \Omega_i)$ such that*

$$\mathbf{q} = \mathbf{a} + \nabla c, \quad (3.3a)$$

$$\|\mathbf{a}\|_{\mathbf{H}_0(\nabla, \Omega_i)} + \|c\|_{H_0(\nabla, \Omega_i)} \lesssim \|\mathbf{q}\|_{H_0(\nabla \times, \Omega_i)}. \quad (3.3b)$$

Theorem 3.4 (Regular decomposition of $H_0(\nabla \cdot, \Omega_i)$). *For any $\mathbf{q} \in H_0(\nabla \cdot, \Omega_i)$, there exist functions $\mathbf{a}, c \in \mathbf{H}_0(\nabla, \Omega_i)$ such that*

$$\mathbf{q} = \mathbf{a} + \nabla \times c, \quad (3.4a)$$

$$\|\mathbf{a}\|_{\mathbf{H}_0(\nabla, \Omega_i)} + \|c\|_{\mathbf{H}_0(\nabla, \Omega_i)} \lesssim \|\mathbf{q}\|_{H_0(\nabla \cdot, \Omega_i)}. \quad (3.4b)$$

Our derivation of the mixed-dimensional regular decomposition relies on the fact that the regular decompositions in above theorems are possible on the individual sub-manifolds Ω_i and then combined together, by taking special care of the traces.

3.2 Mixed-dimensional Regular Decomposition

For $i \in I$, let us first introduce the subspace of k -forms with increased regularity, denoted by $H^1\Lambda^k(\Omega_i) \subseteq H\Lambda^k(\Omega_i)$ such that

$$H^1\Lambda^k(\Omega_i) \cong (H(\nabla, \Omega_i))^{C_{d_i, k}}.$$

Here the notation \cong means that the spaces are isomorphic. The exponent is given by the binomial coefficient $C_{d_i, k} := \binom{d_i}{k}$, which is the dimension of the space of differential k -forms on a d_i -manifold (see e.g. [27], Thm 4-5). We consider the space as zero if the exponent is zero, e.g. if $k > d_i$.

With the local spaces defined, let $H^1\mathfrak{L}^k \subseteq H\mathfrak{L}^k$ be the space of regular mixed-dimensional k -forms, given by

$$H^1\mathfrak{L}^k := \prod_{i \in I} \{a_i \in H^1\Lambda^{k_i}(\Omega_i) : \text{Tr}_j a_i \in H^1\Lambda^{k_i}(\Omega_{i_j}), \forall j \in I_i\}, \quad (3.5)$$

and endowed with the norm

$$\|a\|_{H^1\mathfrak{L}^k} := \sum_{i \in I} \|a_i\|_{H^1\Lambda^{k_i}(\Omega_i)} + \sum_{j \in I_i} \|\text{Tr}_j a_i\|_{H^1\Lambda^{k_i}(\Omega_{i_j})}. \quad (3.6)$$

We note two properties of the space $H^1\mathfrak{L}^k$. First, in the special case of $i \in I^{n-k}$, we have $k_i = 0$. Since $H^1\Lambda^0(\Omega_i) = H\Lambda^0(\Omega_i)$, it follows that

$$\iota_i H^1\mathfrak{L}^k = \iota_i H\mathfrak{L}^k, \quad \forall i \in I^{n-k}. \quad (3.7a)$$

Secondly, the jump operator preserves the increased regularity of $H^1\mathfrak{L}^k$:

$$\mathfrak{d}H^1\mathfrak{L}^k \subseteq H^1\mathfrak{L}^{k+1}. \quad (3.7b)$$

The following lemma provides the local regular decompositions on each Ω_i by using the known results in fixed-dimensional setting in Section 3.1.

Lemma 3.1. *Given $q_i \in \iota_i H\mathfrak{L}^k$ with $i \in I$, then there exists a pair $(a_i, c_i) \in \iota_i H^1\mathfrak{L}^k \times \iota_i H^1\mathfrak{L}^{k-1}$ such that*

$$q_i = a_i + \mathfrak{d}c_i \quad \text{and} \quad \|a_i\|_{H^1\mathfrak{L}^k} + \|c_i\|_{H^1\mathfrak{L}^{k-1}} \lesssim \|q_i\|_{H\mathfrak{L}^k}.$$

Proof. We consider the four possible cases for $n \leq 3$. With reference to diagram (2.5), these cases are represented by the main diagonal (Case A) and the off-diagonal components in the three bottom rows (Cases B–D).

Case A: $k = n - d_i$. We note that this means that $k_i = 0$ and $\iota_i H\mathfrak{L}^k = \iota_i H^1\mathfrak{L}^k$ by (3.7a). Setting $a_i := q_i$ yields the result.

Case B: $k = n$, $d_i > 0$. In this case, we have $q_i \in L^2(\Omega_i)$. We introduce $a_i \in H_0^1(\Omega_i)$ as the solution to the following minimization problem,

$$\min_{a_i \in H_0^1(\Omega_i)} \frac{1}{2} \|a_i\|_{1, \Omega_i}^2 \quad \text{subject to } \Pi_{\mathbb{R}, i} a_i = \Pi_{\mathbb{R}, i} q_i, \quad (3.8a)$$

with $\Pi_{\mathbb{R}, i}$ denoting the L^2 -projection onto constants on Ω_i . Secondly, we define the bounded $c_i \in (H_0^1(\Omega_i))^{d_i}$ such that

$$\nabla \cdot c_i = (I - \Pi_{\mathbb{R}, i})(q_i - a_i). \quad (3.8b)$$

Since the divergence represents the exterior derivative \mathfrak{d} in this case, it follows that $q_i = a_i + \mathfrak{d}c_i$ with $a_i \in \iota_i H^1\mathfrak{L}^k$ and $c_i \in \iota_i H^1\mathfrak{L}^{k-1}$. Importantly, a_i and c_i have zero trace on $\partial\Omega_i$. This property will be advantageous in the remaining cases.

Case C: $k = n - 1$, $d_i > 1$. In this case, we require L^2 regularity of traces on manifolds of codimension one. For $j \in I_i^{d_i-1}$, let us denote

$$q_j := \text{Tr}_j q_i.$$

By definition of $H\mathfrak{L}^{n-1}$, we have that $q_j \in L^2(\Omega_{i_j}) = L^2(\partial_j \Omega_i)$. Since $\partial_j \Omega_i$ is a manifold of dimension $d_i - 1$, we can use Case B to find $a_j \in H_0^1(\partial_j \Omega_i)$ and $c_j \in (H_0^1(\partial_j \Omega_i))^{d_i-1}$ such that

$$q_j = a_j + \mathfrak{d}c_j.$$

Note that both a_j and c_j have zero trace on the boundary of $\partial_j \Omega_i$. Hence, all a_j (respectively c_j) can be combined to form a function in $H^1(\partial \Omega_i)$ (respectively $(H^1(\partial \Omega_i))^{d_i-1}$). These boundary functions are extended harmonically into Ω_i to form $a_i^* \in \iota_i H^1 \mathfrak{L}^k$ and $c_i^* \in \iota_i H^1 \mathfrak{L}^{k-1}$ such that

$$\mathrm{Tr}_j a_i^* = a_j, \quad \mathrm{Tr}_j c_i^* = c_j, \quad \forall j \in I_i^{d_i-1}$$

The regularity of these extensions in the domain Ω_i is a result of the fact that all a_j and c_j are zero at tips and reentrant corners.

Next, we note that $q_i - (a_i^* + \mathrm{dc}_i^*)$ has zero trace on $\partial_j \Omega_i$ for all $j \in I_i^{d_i-1}$. Hence, we apply a regular decomposition respecting homogeneous boundary conditions to obtain

$$q_i - (a_i^* + \mathrm{dc}_i^*) = a_i^0 + \mathrm{dc}_i^0,$$

such that $a_i^0 \in H^1 \Lambda^{k_i}(\Omega_i)$ and $c_i^0 \in H^1 \Lambda^{k_i-1}(\Omega_i)$ have zero trace on each $\partial_j \Omega_i$ with $j \in I_i^{d_i-1}$. It follows that $a_i^0 \in \iota_i H^1 \mathfrak{L}^k$ and $c_i^0 \in \iota_i H^1 \mathfrak{L}^{k-1}$. We conclude the construction by setting $a_i := a_i^* + a_i^0$ and $c_i := c_i^* + c_i^0$.

Case D: $k = n - 2$, $d_i > 2$. The only case not covered so far is $d_i = n = 3$. Following the same arguments as above, we first denote $q_j := \mathrm{Tr}_j q_i$ and then use the construction from Case C to obtain

$$q_j = a_j + \mathrm{dc}_j, \quad j \in I_i^2.$$

Next, without loss of generality, we let $j_1, j_2 \in I_i^2$ and consider the index $j_{1,2} \in I_i^1$ such that $\partial_{j_{1,2}} \Omega_i$ forms a one-dimensional interface between $\partial_{j_1} \Omega_i$ and $\partial_{j_2} \Omega_i$. It follows that

$$\mathrm{Tr}_{j_{1,2}} a_{j_1} = \mathrm{Tr}_{j_{1,2}} a_{j_2} \quad \mathrm{Tr}_{j_{1,2}} c_{j_1} = \mathrm{Tr}_{j_{1,2}} c_{j_2}$$

since both traces are equal to the unique constructions on $\partial_{j_{1,2}} \Omega_i$ from Case B, in particular (3.8). This means that, when there are more interfaces, by combining all a_j with $j \in I_i^2$, a function is formed in $(H^1(\partial \Omega_i))^2$. Analogously, the combination of all c_j with $j \in I_i^2$ forms a function in $H^1(\partial \Omega_i)$.

The construction is finalized in the same way as in Case C. In short, we first introduce a harmonic extension of the boundary functions to form $a_i^* \in \iota_i H^1 \mathfrak{L}^k$ and $c_i^* \in \iota_i H^1 \mathfrak{L}^{k-1}$. Then, $a_i^0 \in \iota_i H^1 \mathfrak{L}^k$ and $c_i^0 \in \iota_i H^1 \mathfrak{L}^{k-1}$ are constructed using a regular decomposition of $q_i - (a_i^* + \mathrm{dc}_i^*)$ respecting homogeneous boundary conditions. Finally, we set $a_i := a_i^* + a_i^0$ and $c_i := c_i^* + c_i^0$.

□

Remark 3.1. In the previous lemma, we have frequently used the fact that operators Tr and $\mathrm{d}\mathbf{c}$ commute. The derivation of this property for functions on each Ω_i is straightforward so, to shorten the presentation, we leave it out and use the commutative property in the proofs when needed.

Now we are ready to present the main result of this section, namely the mixed-dimensional regular decomposition, in the following theorem.

Theorem 3.5 (Mixed-dimensional Regular Decomposition). *Given $\mathbf{q} \in H \mathfrak{L}^k$, then there exists a pair $(\mathbf{a}, \mathbf{c}) \in H^1 \mathfrak{L}^k \times H^1 \mathfrak{L}^{k-1}$ such that*

$$\mathbf{q} = \mathbf{a} + \mathrm{d}\mathbf{c} \quad \text{and} \quad \|\mathbf{a}\|_{H^1 \mathfrak{L}^k} + \|\mathbf{c}\|_{H^1 \mathfrak{L}^{k-1}} \lesssim \|\mathbf{q}\|_{H \mathfrak{L}^k}$$

Proof. Given k , we construct $\mathbf{a} = (a_i)_{i \in I}$ and $\mathbf{c} = (c_i)_{i \in I}$ by marching through the corresponding row in diagram (2.5). We initialize both functions as $\mathbf{a} = 0$ and $\mathbf{c} = 0$, and redefine each component according to the following four, sequential steps.

1. If $k > 0$, consider $i \in I^n$. Lemma 3.1 gives us $a_i \in \iota_i H^1 \mathfrak{L}^k$ and $c_i \in \iota_i H^1 \mathfrak{L}^{k-1}$ such that

$$q_i = a_i + \mathrm{dc}_i. \quad (3.9a)$$

We repeat the above for all $i \in I^n$ and continue with step 2.

2. If $k > 1$, consider $i \in I^{n-1}$. We use Lemma 3.1 to define $\tilde{a}_i \in \iota_i H^1 \mathfrak{L}^k$ and $c_i \in \iota_i H^1 \mathfrak{L}^{k-1}$ such that

$$q_i = \tilde{a}_i + \mathrm{d}c_i.$$

Noting that $(q_i - \mathrm{d}c_i) \in \iota_i H^1 \mathfrak{L}^k$ and using (3.7b), we set

$$a_i := q_i - \mathrm{d}c_i - \iota_i \mathfrak{d}\mathfrak{c}. \quad (3.9b)$$

where \mathfrak{c} has non-zero components c_j , $j \in I^n$ defined in step 1. We repeat this construction for all $i \in I^{n-1}$ and continue with step 3.

3. If $k > 2$, repeat step 2 with $i \in I^{n-2}$ and continue with step 4.
 4. In any case, consider $i \in I^{n-k}$. We have $k_i = 0$ and note that $\iota_i H \mathfrak{L}^k = \iota_i H^1 \mathfrak{L}^k$ from (3.7a). Hence, we use (3.7b) to set

$$a_i := q_i - \iota_i \mathfrak{d}\mathfrak{c}. \quad (3.9c)$$

where \mathfrak{c} has non-zero components defined in steps 1–3. This construction is repeated for all $i \in I^{n-k}$.

The four steps give us $\mathfrak{a} := (a_i)_{i \in I} \in H^1 \mathfrak{L}^k$ and $\mathfrak{c} := (c_i)_{i \in I} \in H^1 \mathfrak{L}^{k-1}$ and we collect (3.9) to conclude

$$\mathfrak{q} = \mathfrak{a} + \mathfrak{d}\mathfrak{c}.$$

The bound follows by the construction and Lemma 3.1. \square

A byproduct of the mixed-dimensional regular decomposition is the so-called regular inverse of the mixed-dimensional differential \mathfrak{d} as shown in the following corollary.

Corollary 3.1 (Mixed-dimensional Regular Inverse). *Given $\mathfrak{q} \in H \mathfrak{L}^k$, then there exists $\mathfrak{a} \in H^1 \mathfrak{L}^k$ such that*

$$\mathfrak{d}(\mathfrak{q} - \mathfrak{a}) = 0 \quad \text{and} \quad \|\mathfrak{a}\|_{H^1 \mathfrak{L}^k} \lesssim \|\mathfrak{q}\|_{H \mathfrak{L}^k}$$

Proof. Follows from Theorem 3.5 and the fact that $\mathfrak{d}\mathfrak{d}\mathfrak{c} = 0$ from (2.3). \square

4 Discrete Regular Decomposition

In this section, we introduce the discrete version of the regular decomposition (Theorem 3.5). To this end, let h be the typical mesh size and the subscript h describe discrete entities. We first present the conventional discrete regular decomposition in a fixed-dimensional setting. Then, we introduce the structure-preserving discretization of the mixed-dimensional geometry Ω and function spaces $H \mathfrak{L}^k$. We finalize the section with deriving the discrete mixed-dimensional regular decomposition.

4.1 Fixed-dimensional Discrete Regular Decomposition

Let $H_h(\nabla, \Omega_i)$, $H_h(\nabla \times, \Omega_i)$, and $H_h(\nabla \cdot, \Omega_i)$ denote the conforming finite element approximations of the functions spaces $H(\nabla, \Omega_i)$, $H(\nabla \times, \Omega_i)$ and $H(\nabla \cdot, \Omega_i)$. In addition, let $\Pi_h^{\nabla \times} : H(\nabla \times, \Omega_i) \rightarrow H_h(\nabla \times, \Omega_i)$ and $\Pi_h^{\nabla \cdot} : H(\nabla \cdot, \Omega_i) \rightarrow H_h(\nabla \cdot, \Omega_i)$ be the stable projection operators. In connection to Section 3.1, the discrete analogues of Theorem 3.1 and Theorem 3.2 are given below.

Theorem 4.1 (Regular decomposition of $H_h(\nabla \times, \Omega_i)$). *For any $\mathbf{q}_h \in H_h(\nabla \times, \Omega_i)$, there exist vector functions $\mathbf{a}_h \in (H_h(\nabla, \Omega_i))^3$, $\mathbf{b}_h \in H_h(\nabla \times, \Omega_i)$ and a scalar function $c_h \in H_h(\nabla, \Omega_i)$ such that*

$$\mathbf{q}_h = \Pi_h^{\nabla \times} \mathbf{a}_h + \mathbf{b}_h + \nabla c_h, \quad (4.1a)$$

$$\|\Pi_h^{\nabla \times} \mathbf{a}_h\|_{H(\nabla \times, \Omega_i)} + \|h^{-1} \mathbf{b}_h\|_{L^2(\Omega_i)} + \|c_h\|_{H(\nabla, \Omega_i)} \lesssim \|\mathbf{q}_h\|_{H(\nabla \times, \Omega_i)}. \quad (4.1b)$$

Theorem 4.2 (Regular decomposition of $H_h(\nabla \cdot, \Omega_i)$). *For any $\mathbf{q}_h \in H_h(\nabla \cdot, \Omega_i)$, there exist vector functions $\mathbf{a}_h, \mathbf{e}_h \in (H_h(\nabla, \Omega_i))^3$, $\mathbf{b}_h \in H_h(\nabla \cdot, \Omega_i)$ and $\mathbf{f}_h \in H_h(\nabla \times, \Omega_i)$ such that*

$$\mathbf{q}_h = \Pi_h^{\nabla \cdot} \mathbf{a}_h + \mathbf{b}_h + \nabla \times (\Pi_h^{\nabla \times} \mathbf{e}_h + \mathbf{f}_h), \quad (4.2a)$$

$$\|\Pi_h^{\nabla \cdot} \mathbf{a}_h\|_{H(\nabla \cdot, \Omega_i)} + \|h^{-1} \mathbf{b}_h\|_{L^2(\Omega_i)} + \|\mathbf{e}_h\|_{H(\nabla \times, \Omega_i)} + \|h^{-1} \mathbf{f}_h\|_{L^2(\Omega_i)} \lesssim \|\mathbf{q}_h\|_{H(\nabla \cdot, \Omega_i)}. \quad (4.2b)$$

These discrete regular decompositions reveal the structure that we aim to preserve in the mixed-dimensional setting. Specifically, the stability of the decompositions in the sense of bounds (4.1b) and (4.2b) will in turn provide us with robust preconditioners by the theory of the auxiliary space methods. We give a short overview of the auxiliary space preconditioning theory later in Section 5.1 and focus first on the derivation of the mixed-dimensional analogue to Theorem 4.1 and Theorem 4.2.

4.2 Mixed-dimensional Discretization

First, we introduce a shape-regular simplicial partition of Ω , denoted by $\Omega_h = \bigcup_{i \in I} \Omega_{i,h}$. The grid is constructed such that it conforms to all lower-dimensional manifolds and all grids are matching. In order to preserve the regular decomposition on the discrete level, structure preserving discretization in the mixed-dimensional setting should be considered. Let us introduce $H_h \mathfrak{L}^k$ as the discretization of $H \mathfrak{L}^k$ defined on Ω_h . Using the notation of finite element exterior calculus [4], we consider the family of reduced finite elements (i.e. elements of the first kind) and set

$$H_h \mathfrak{L}^k = \prod_{i \in I} P_r^- \Lambda^{k_i}(\Omega_{i,h}). \quad (4.3)$$

The lowest-order case ($r = 1$) in the three-dimensional setting ($n = 3$) gives us the following, discrete de Rham complex:

$$\begin{array}{ccccccc} H_h \mathfrak{L}^0 & & \mathbb{P}_1(\Omega_h^3) & & & & \\ \downarrow \mathfrak{d} & & \downarrow \nabla & \searrow \mathfrak{d} & & & \\ H_h \mathfrak{L}^1 & & \mathbb{N}_0^e(\Omega_h^3) & & \mathbb{P}_1(\Omega_h^2) & & \\ \downarrow \mathfrak{d} & & \downarrow \nabla \times & \searrow \mathfrak{d} & \downarrow \nabla^\perp & \searrow \mathfrak{d} & \\ H_h \mathfrak{L}^2 & & \mathbb{N}_0^f(\Omega_h^3) & & \mathbb{RT}_0(\Omega_h^2) & & \mathbb{P}_1(\Omega_h^1) \\ \downarrow \mathfrak{d} & & \downarrow \nabla \cdot & \searrow \mathfrak{d} & \downarrow \nabla \cdot & \searrow \mathfrak{d} & \downarrow \nabla \cdot \\ H_h \mathfrak{L}^3 & & \mathbb{P}_0(\Omega_h^3) & & \mathbb{P}_0(\Omega_h^2) & & \mathbb{P}_0(\Omega_h^1) & & \mathbb{P}_0(\Omega_h^0) \end{array} \quad (4.4)$$

Here, \mathbb{P}_1 , \mathbb{RT}_0 , and \mathbb{P}_0 denote linear Lagrange, lowest-order Raviart-Thomas, and piecewise constant finite element spaces, respectively. \mathbb{N}_0^e and \mathbb{N}_0^f represent the edge-based and face-based Nédélec elements of lowest order, respectively.

We introduce the stable projection operators $\Pi_h^k : H \mathfrak{L}^k \mapsto H_h \mathfrak{L}^k$ such that

$$\|(I - \Pi_h^k) \mathbf{a}\|_{L^2 \mathfrak{L}^k} \lesssim h \|\mathbf{a}\|_{H^1 \mathfrak{L}^k}, \quad \forall \mathbf{a} \in H^1 \mathfrak{L}^k, \quad (4.5)$$

and the following diagram commutes,

$$\begin{array}{ccccccc} H \mathfrak{L}^0 & \xrightarrow{\mathfrak{d}} & H \mathfrak{L}^1 & \xrightarrow{\mathfrak{d}} & H \mathfrak{L}^2 & \xrightarrow{\mathfrak{d}} & H \mathfrak{L}^3 \\ \downarrow \Pi_h^0 & & \downarrow \Pi_h^1 & & \downarrow \Pi_h^2 & & \downarrow \Pi_h^3 \\ H_h \mathfrak{L}^0 & \xrightarrow{\mathfrak{d}} & H_h \mathfrak{L}^1 & \xrightarrow{\mathfrak{d}} & H_h \mathfrak{L}^2 & \xrightarrow{\mathfrak{d}} & H_h \mathfrak{L}^3 \end{array} \quad (4.6)$$

In the mixed-dimensional setting, such a bounded projection can be constructed by combining fixed-dimensional cochain projections on each Ω_i together. For the construction of fixed-dimensional cochain projections, we refer to [11].

Lemma 4.1 (Exactness). *Given the commuting projection operators Π_h^k exist, then all discrete closed forms are exact. Thus, for each $\mathbf{q}_h \in H_h \mathfrak{L}^k$ with $\mathfrak{d}\mathbf{q}_h = 0$, there exists a $\mathbf{c}_h \in H_h \mathfrak{L}^{k-1}$ such that*

$$\mathfrak{d}\mathbf{c}_h = \mathbf{q}_h.$$

Proof. Assume $\mathbf{q}_h \in H_h \mathfrak{L}^k$ with $\mathfrak{d}\mathbf{q}_h = 0$ given. Since $H_h \mathfrak{L}^k \subset H \mathfrak{L}^k$, we use the exactness of the mixed-dimensional De Rham complex (2.4) to find $\mathbf{c} \in H \mathfrak{L}^{k-1}$ such that

$$\mathfrak{d}\mathbf{c} = \mathbf{q}_h.$$

Setting $\mathbf{c}_h := \Pi_h^{k-1} \mathbf{c}$, we obtain

$$\mathfrak{d}\mathbf{c}_h = \mathfrak{d}\Pi_h^{k-1} \mathbf{c} = \Pi_h^k \mathfrak{d}\mathbf{c} = \Pi_h^k \mathbf{q}_h = \mathbf{q}_h,$$

which completes the proof. \square

4.3 Mixed-dimensional Discrete Regular Decomposition

This section is devoted to deriving the discrete regular decomposition, i.e. the discrete analogue to Theorem 3.5. We first require the following preparatory lemma.

Lemma 4.2. *Given $\mathbf{q}_h \in H_h \mathfrak{L}^k$, then there exists a semi-discrete pair $(\mathbf{a}, \mathbf{f}_h) \in H^1 \mathfrak{L}^k \times H_h \mathfrak{L}^{k-1}$ such that*

$$\mathbf{q}_h = \Pi_h^k \mathbf{a} + \mathfrak{d}\mathbf{f}_h \quad \text{and} \quad \|\mathbf{a}\|_{H^1 \mathfrak{L}^k} + \|\mathbf{f}_h\|_{H \mathfrak{L}^{k-1}} \lesssim \|\mathbf{q}_h\|_{H \mathfrak{L}^k}.$$

Proof. Since $\mathbf{q}_h \in H_h \mathfrak{L}^k \subset H \mathfrak{L}^k$, we use Corollary 3.1 to construct $\mathbf{a} \in H^1 \mathfrak{L}^k$ such that

$$\mathfrak{d}(\mathbf{q}_h - \mathbf{a}) = 0$$

Next, we use $\mathfrak{d}H_h \mathfrak{L}^k \subseteq H_h \mathfrak{L}^{k+1}$ and the commutativity of the projection operators to derive

$$\mathfrak{d}\mathbf{q}_h = \Pi_h^{k+1} \mathfrak{d}\mathbf{q}_h = \Pi_h^{k+1} \mathfrak{d}\mathbf{a} = \mathfrak{d}\Pi_h^k \mathbf{a}.$$

We thus have $\mathfrak{d}(\mathbf{q}_h - \Pi_h^k \mathbf{a}) = 0$, i.e. $\mathbf{q}_h - \Pi_h^k \mathbf{a}$ is a closed form in $H_h \mathfrak{L}^k$. From Lemma 4.1, a $\mathbf{f}_h \in H_h \mathfrak{L}^{k-1}$ exists such that

$$\mathfrak{d}\mathbf{f}_h = \mathbf{q}_h - \Pi_h^k \mathbf{a}.$$

By Corollary 3.1, we have $\|\mathbf{a}\|_{H^1 \mathfrak{L}^k} \lesssim \|\mathbf{q}_h\|_{H \mathfrak{L}^k}$. In addition, by (4.5), we have

$$\begin{aligned} \|\mathfrak{d}\mathbf{f}_h\|_{L^2 \mathfrak{L}^k} &\lesssim \|\mathbf{q}_h\|_{L^2 \mathfrak{L}^k} + \|\Pi_h^k \mathbf{a}\|_{L^2 \mathfrak{L}^k} \leq \|\mathbf{q}_h\|_{L^2 \mathfrak{L}^k} + \|\mathbf{a}\|_{L^2 \mathfrak{L}^k} + \|(I - \Pi_h^k) \mathbf{a}\|_{L^2 \mathfrak{L}^k} \\ &\lesssim \|\mathbf{q}_h\|_{L^2 \mathfrak{L}^k} + \|\mathbf{a}\|_{H^1 \mathfrak{L}^k} \lesssim \|\mathbf{q}_h\|_{H \mathfrak{L}^k}. \end{aligned}$$

Since the choice of \mathbf{f}_h is not unique, we choose a special \mathbf{f}_h such that the following Poincaré inequality holds

$$\|\mathbf{f}_h\|_{H \mathfrak{L}^{k-1}} \lesssim \|\mathfrak{d}\mathbf{f}_h\|_{L^2 \mathfrak{L}^k}.$$

Then we have $\|\mathbf{f}_h\|_{H \mathfrak{L}^{k-1}} \lesssim \|\mathbf{q}_h\|_{H \mathfrak{L}^k}$, which completes the proof. \square

To further develop the decomposition in the discrete setting, let us introduce $H_h^1 \mathfrak{L}^k \subseteq H^1 \mathfrak{L}^k$ as the discretization of the regular k -forms from (3.5). For the given choice of discrete spaces (4.3), the regular spaces are given by

$$H_h^1 \mathfrak{L}^k = \prod_{i \in I} (P_r^- \Lambda^0(\Omega_{i,h}))^{C_{d_i, k_i}}.$$

Again, the exponent is given by $C_{d_i, k_i} := \binom{d_i}{k_i}$. In the lowest-order case with $r = 1$, this means that

$$H_h^1 \mathfrak{L}^k = \prod_{i \in I} (\mathbb{P}_1(\Omega_{i,h}))^{C_{d_i, k_i}}.$$

In other words, all discrete forms with increased regularity are given by (tuples of) nodal Lagrange elements. Similar to (3.7), we note that

$$\iota_i H_h^1 \mathfrak{L}^k = \iota_i H_h \mathfrak{L}^k, \quad i \in I^{n-k}, \quad (4.7a)$$

$$\mathfrak{d}H_h^1 \mathfrak{L}^k \subseteq H_h^1 \mathfrak{L}^{k+1}. \quad (4.7b)$$

Let \mathcal{P}_h^k be the projection operator onto the discretized space of regular k -forms. $\mathcal{P}_h^k : H^1 \mathfrak{L}^k \mapsto H_h^1 \mathfrak{L}^k$ is stable and has the following property:

$$\|\mathcal{P}_h^k \mathbf{a}\|_{H^1 \mathfrak{L}^k} \lesssim \|\mathbf{a}\|_{H^1 \mathfrak{L}^k}, \quad \|(I - \mathcal{P}_h^k) \mathbf{a}\|_{L^2 \mathfrak{L}^k} \lesssim h \|\mathbf{a}\|_{H^1 \mathfrak{L}^k}, \quad (4.8)$$

for all $\mathbf{a} \in H^1 \mathfrak{L}^k$. Now we are ready to present the mixed-dimensional discrete regular decomposition as follows.

Theorem 4.3 (Mixed-dimensional Discrete Regular Decomposition). *Given $\mathbf{q}_h \in H_h \mathfrak{L}^k$, then there exists a pair $(\mathbf{a}_h, \mathbf{f}_h) \in H_h^1 \mathfrak{L}^k \times H_h \mathfrak{L}^{k-1}$ and a high-frequency term $\mathbf{b}_h \in H_h \mathfrak{L}^k$ such that*

$$\mathbf{q}_h = \Pi_h^k \mathbf{a}_h + \mathbf{b}_h + \mathfrak{d}\mathbf{f}_h \quad \text{and} \quad \|\mathbf{a}_h\|_{H^1 \mathfrak{L}^k} + \|h^{-1} \mathbf{b}_h\|_{L^2 \mathfrak{L}^k} + \|\mathbf{f}_h\|_{H \mathfrak{L}^{k-1}} \lesssim \|\mathbf{q}_h\|_{H \mathfrak{L}^k}.$$

Proof. Given the decomposition from Lemma 4.2, we further decompose \mathbf{a} using the projection operator \mathcal{P}_h^k from (4.8):

$$\mathbf{q}_h = \Pi_h^k \mathcal{P}_h^k \mathbf{a} + \Pi_h^k (I - \mathcal{P}_h^k) \mathbf{a} + \mathfrak{d}\mathbf{f}_h.$$

By defining $\mathbf{a}_h := \mathcal{P}_h^k \mathbf{a}$ and $\mathbf{b}_h := \Pi_h^k (I - \mathcal{P}_h^k) \mathbf{a}$, we obtain the desired format. To prove the boundedness, we use the stability of \mathcal{P}_h^k and approximation properties (4.5) and (4.8) to derive

$$\begin{aligned} \|\mathbf{a}_h\|_{H^1 \mathfrak{L}^k} &= \|\mathcal{P}_h^k \mathbf{a}\|_{H^1 \mathfrak{L}^k} \lesssim \|\mathbf{a}\|_{H^1 \mathfrak{L}^k} \lesssim \|\mathbf{q}_h\|_{H \mathfrak{L}^k}, \\ \|h^{-1} \mathbf{b}_h\|_{L^2 \mathfrak{L}^k} &= \|h^{-1} \Pi_h^k (I - \mathcal{P}_h^k) \mathbf{a}\|_{L^2 \mathfrak{L}^k} \lesssim \|h^{-1} (I - \mathcal{P}_h^k) \mathbf{a}\|_{L^2 \mathfrak{L}^k} + \|h^{-1} (I - \Pi_h^k) (I - \mathcal{P}_h^k) \mathbf{a}\|_{L^2 \mathfrak{L}^k} \\ &\lesssim \|\mathbf{a}\|_{H^1 \mathfrak{L}^k} + \|(I - \mathcal{P}_h^k) \mathbf{a}\|_{H^1 \mathfrak{L}^k} \lesssim \|\mathbf{a}\|_{H^1 \mathfrak{L}^k}. \end{aligned}$$

Combining these estimates with the bound of Lemma 4.2 proves the result. \square

In practice, it is useful to integrate discrete regular decompositions so that all the components have improved regularity except the high-frequency parts. Such a result is shown as follows.

Corollary 4.1 (Integrated Mixed-dimensional Discrete Regular Decomposition). *Given $\mathbf{q}_h \in H_h \mathfrak{L}^k$, then there exist a regular pair $(\mathbf{a}_h, \mathbf{c}_h) \in H_h^1 \mathfrak{L}^k \times H_h^1 \mathfrak{L}^{k-1}$ and a high-frequency pair $(\mathbf{b}_h, \mathbf{e}_h) \in H_h \mathfrak{L}^k \times H_h \mathfrak{L}^{k-1}$ such that*

$$\Pi_h^k \mathbf{a}_h + \mathbf{b}_h + \mathfrak{d}(\Pi_h^{k-1} \mathbf{c}_h + \mathbf{e}_h) = \mathbf{q}_h \quad (4.9a)$$

$$\|\mathbf{a}_h\|_{H^1 \mathfrak{L}^k} + \|h^{-1} \mathbf{b}_h\|_{L^2 \mathfrak{L}^k} + \|\mathbf{c}_h\|_{H^1 \mathfrak{L}^{k-1}} + \|h^{-1} \mathbf{e}_h\|_{L^2 \mathfrak{L}^{k-1}} \lesssim \|\mathbf{q}_h\|_{H \mathfrak{L}^k}. \quad (4.9b)$$

Proof. Since $H_h^1 \mathfrak{L}^0 = H_h \mathfrak{L}^0$ by (4.7a), the result is trivial for $k = 0$. We use the same argument in combination with Lemma 4.3 to conclude that the case $k = 1$ follows with $\mathbf{e}_h = 0$.

We continue with $k > 1$. Using the decomposition from Lemma 4.3, we obtain $(\mathbf{a}_h, \mathbf{b}_h, \mathbf{f}_h) \in H_h^1 \mathfrak{L}^k \times H_h \mathfrak{L}^k \times H_h \mathfrak{L}^{k-1}$ such that

$$\mathbf{q}_h = \Pi_h^k \mathbf{a}_h + \mathbf{b}_h + \mathfrak{d}\mathbf{f}_h,$$

with the associated bound. Applying Lemma 4.3 once more on $\mathbf{f}_h \in H_h \mathfrak{L}^{k-1}$, we have $(\mathbf{c}_h, \mathbf{e}_h, \mathbf{g}_h) \in H_h^1 \mathfrak{L}^{k-1} \times H_h \mathfrak{L}^{k-1} \times H_h \mathfrak{L}^{k-2}$ such that

$$\mathbf{f}_h = \Pi_h^{k-1} \mathbf{c}_h + \mathbf{e}_h + \mathfrak{d}\mathbf{g}_h$$

Due to (2.3), we have $\mathfrak{d}\mathfrak{d}\mathbf{g}_h = 0$ and the result follows. \square

Similarly, in the discrete case, we also have the regular inverse as the byproduct of the discrete regular decomposition, which is stated in the following corollary.

Corollary 4.2 (Discrete Regular Inverse). *Given $\mathbf{q}_h \in H_h \mathfrak{L}^k$, then there exist $\mathbf{a}_h \in H_h^1 \mathfrak{L}^k$ and a high-frequency term $\mathbf{b}_h \in H_h \mathfrak{L}^k$ such that*

$$\mathfrak{d}(\mathbf{q}_h - \Pi_h^k \mathbf{a}_h - \mathbf{b}_h) = 0 \quad \text{and} \quad \|\mathbf{a}_h\|_{H^1 \mathfrak{L}^k} + \|h^{-1} \mathbf{b}_h\|_{L^2 \mathfrak{L}^k} \lesssim \|\mathbf{q}_h\|_{H \mathfrak{L}^k} \quad (4.10)$$

Proof. Follows from Theorem 4.1 and the fact that $\mathfrak{d}\mathfrak{d} = 0$ from (2.3). \square

5 Mixed-dimensional Auxiliary Space Preconditioner

Based on the (discrete) regular decomposition, we develop robust preconditioners for solving the following abstract mixed-dimensional problem: Find $\mathbf{q}_h \in H_h \mathfrak{L}^k$, such that

$$(\mathbf{q}_h, \tilde{\mathbf{q}}_h)_{L^2 \mathfrak{L}^k} + (\mathfrak{d}\mathbf{q}_h, \mathfrak{d}\tilde{\mathbf{q}}_h)_{L^2 \mathfrak{L}^{k+1}} = (\mathfrak{f}, \tilde{\mathbf{q}}_h)_{L^2 \mathfrak{L}^k} \quad \forall \tilde{\mathbf{q}}_h \in H_h \mathfrak{L}^k. \quad (5.1)$$

This can be written into a linear system $\mathfrak{A}^k \mathbf{q}_h = \mathfrak{f}$, where $\mathfrak{A}^k = \mathfrak{I} + \mathfrak{d}^* \mathfrak{d}$ is a symmetric positive definite operator on $H_h \mathfrak{L}^k$, \mathfrak{I} is the identity mapping and \mathfrak{d}^* is the adjoint of \mathfrak{d} . Our goal is to derive a preconditioner \mathfrak{B} for the problem (5.1) based on the fictitious or auxiliary space preconditioning theory developed in [16, 24, 29].

5.1 Abstract Theory of Auxiliary Space Preconditioning

We recall the framework of the auxiliary space theory. Assume V is a separable Hilbert space with an inner product $a(\cdot, \cdot)$. We aim to find $u \in V$ that solves

$$a(u, v) = (f, v) \quad \forall v \in V, \quad (5.2)$$

or equivalently

$$Au = f, \quad (5.3)$$

where $A : V \mapsto V'$ is symmetric positive definite such that $\langle Au, v \rangle = a(u, v)$. Here V' is the dual of V . Using A , the norm induced by $a(\cdot, \cdot)$ can be denoted by $\|\cdot\|_A$ and we also consider another inner product $s(\cdot, \cdot)$ on V , which induces another norm $\|\cdot\|_S$ with S being symmetric positive definite.

For designing auxiliary preconditioners, let W_ℓ , $\ell = 1, 2, \dots, L$, be auxiliary spaces with inner products $a_\ell(\cdot, \cdot)$ that induces norms $\|\cdot\|_{A_\ell}$, where $A_\ell : W_\ell \mapsto W'_\ell$ are linear operators defined as $\langle A_\ell u_\ell, v_\ell \rangle = a_\ell(u_\ell, v_\ell)$, for $u_\ell, v_\ell \in W_\ell$, $\ell = 1, 2, \dots, L$. In addition, we assume that there are transfer operators $\Pi_\ell : W_\ell \mapsto V$. Finally, we define the auxiliary product space $\bar{V} = V \times W_1 \times W_2 \times \dots \times W_L$, and then represent the inner product on \bar{V} as

$$\bar{a}(\bar{v}, \bar{v}) = s(v, v) + \sum_{\ell=1}^L a_\ell(w_\ell, w_\ell) \quad \forall \bar{v} = (v, w_1, \dots, w_L) \in \bar{V}.$$

Using the fictitious or auxiliary space method, the preconditioner $B : V' \mapsto V$ for the linear problem (5.3) is defined as

$$B = S^{-1} + \sum_{\ell=1}^L \Pi_\ell A_\ell^{-1} \Pi_\ell^*, \quad (5.4)$$

where S^{-1} is the so-called smoother operator. The following Lemma from [16], which can be viewed as a special case of the fictitious lemma [24], gives a bound on the condition number $\kappa(BA)$.

Lemma 5.1. *Assume the following conditions hold:*

1. *There exist $c_\ell > 0$, $\ell = 1, \dots, L$ such that $\|\Pi_\ell w_\ell\|_A \leq c_\ell \|w_\ell\|_{A_\ell}$, $\forall w_\ell \in W_\ell$.*
2. *There exist $c_s > 0$ such that $\|v\|_A \leq c_s \|v\|_S$, $\forall v \in V$.*
3. *For every $v \in V$, there exists a decomposition $v = v_0 + \sum_{\ell=1}^L w_\ell$, $v_0 \in V$, $w_\ell \in W_\ell$ and $c_0 > 0$ such that*

$$\|v_0\|_S^2 + \sum_{\ell=1}^L \|w_\ell\|_{A_\ell}^2 \leq c_0 \|v\|_A^2.$$

Then $\kappa(BA) \leq c_0^2(c_s^2 + c_1^2 + \dots + c_L^2)$.

If all the bounds in Lemma 5.1 are independent of discretization parameter h (and any other parameters), then B is a robust preconditioner for A in (5.3). The auxiliary space preconditioner B (5.4) can be viewed as additive version. As mentioned in [16], naturally, we can also apply auxiliary spaces successively to obtain a multiplicative auxiliary space preconditioner, which is also robust under the same conditions, we refer to [17] for details. Note that instead of directly applying operators A_ℓ^{-1} , we can replacing them by their spectrally equivalent approximations, B_ℓ . As long as the constants in the spectral equivalence are independent of physical and discretization parameters, the resulting auxiliary space preconditioners remain robust.

Remark 5.1. For example, [16] shows that the fixed-dimensional discrete regular decomposition in Theorem 4.2 follows the conditions of Lemma 5.1. Let $V = H_h(\nabla \cdot, \Omega_i)$ and for $u, v \in V$ let the bilinear form $a(u, v) = (u, v) + (\nabla \cdot u, \nabla \cdot v)$ in (5.2). The auxiliary space theory gives the following preconditioner for solving (5.3). Take the auxiliary spaces $W_1 = (H_h(\nabla, \Omega_i))^3$, $W_2 = H_h(\nabla \times, \Omega_i)$, $W_3 = (H_h(\nabla, \Omega_i))^3$ and transfer operators $\Pi_1 = \Pi_h^{\nabla \cdot}$, $\Pi_2 = \nabla \times$, $\Pi_3 = \nabla \times \Pi_h^{\nabla \times}$. With certain choices of smoothers $S^{\nabla \cdot}$ and $S^{\nabla \times}$ on $H_h(\nabla \cdot, \Omega_i)$ and $H_h(\nabla \times, \Omega_i)$ (for example, Jacobi smoother), respectively, we get

$$B = (S^{\nabla \cdot})^{-1} + \Pi_h^{\nabla \cdot} A_{reg}^{-1} (\Pi_h^{\nabla \cdot})^* + \nabla \times (S^{\nabla \times})^{-1} (\nabla \times)^* + \nabla \times \Pi_h^{\nabla \times} A_{reg}^{-1} (\nabla \times \Pi_h^{\nabla \times})^*, \quad (5.5)$$

where A_{reg} is the linear operator induced by the inner product on $(H_h(\nabla, \Omega_i))^3$. In the following section, we show that the similar preconditioner is feasible in the mixed-dimensional setting using Theorem 4.3.

5.2 Mixed-dimensional Preconditioner

Let us apply the theory in Section 5.1 on the problem (5.1) to develop the auxiliary space preconditioner in the mixed-dimensional setting. Following Theorem 4.3, for any $\mathbf{q}_h \in H_h \mathfrak{L}^k$, there is a pair $(\mathbf{a}_h, \mathbf{f}_h) \in H_h^1 \mathfrak{L}^k \times H_h \mathfrak{L}^{k-1}$ and a high-frequency term $\mathbf{b}_h \in H_h \mathfrak{L}^k$ that allows the following decomposition

$$\mathbf{q}_h = \mathbf{b}_h + \Pi_h^k \mathbf{a}_h + \mathfrak{d} \mathbf{f}_h.$$

Now, besides the original space $V = H_h \mathfrak{L}^k$, we have two auxiliary spaces $W_1 = H_h^1 \mathfrak{L}^k$ and $W_2 = H_h \mathfrak{L}^{k-1}$. Furthermore, we take the transfer operator $\Pi_1 = \Pi_h^k$ restricted to $H_h^1 \mathfrak{L}^k$, i.e. $\Pi_h^k : H_h^1 \mathfrak{L}^k \mapsto H_h \mathfrak{L}^k$, and $\Pi_2 = \mathfrak{d}$. We write \mathfrak{A}_{reg}^k for the symmetric positive definite linear operator defined by the inner product on the space $H^1 \mathfrak{L}^k$, which can be viewed as (vector) Laplacian operators in the mixed-dimensional setting.

For the sake of simplicity, we consider the Jacobi smoother. For a function $\mathbf{q}_h \in H_h \mathfrak{L}^k$, we have $\mathbf{q}_h = \sum_{\mathfrak{e}} \mathbf{q}_h^{\mathfrak{e}}$, where $\mathbf{q}_h^{\mathfrak{e}} \in \text{span}\{\mathfrak{e}\}$ where \mathfrak{e} denotes a degree of freedom defined on either a node, edge, face or cell of Ω_h . Then the smoothing operator is characterized by the inner product

$$s(\mathbf{q}_h, \mathbf{q}_h) = \sum_{\mathfrak{e}} ((\mathbf{q}_h^{\mathfrak{e}}, \mathbf{q}_h^{\mathfrak{e}})_{L^2 \mathfrak{L}^k} + (\mathfrak{d} \mathbf{q}_h^{\mathfrak{e}}, \mathfrak{d} \mathbf{q}_h^{\mathfrak{e}})_{L^2 \mathfrak{L}^{k+1}}).$$

This leads to a smoother \mathfrak{S}^k , which, in matrix representation, coincides with the diagonal of \mathfrak{A}^k .

The auxiliary space preconditioner $\mathfrak{B} : (H_h \mathfrak{L}^k)' \mapsto H_h \mathfrak{L}^k$ for (5.1) takes the following form

$$\mathfrak{B}^k = (\mathfrak{S}^k)^{-1} + \Pi_h^k (\mathfrak{A}_{reg}^k)^{-1} (\Pi_h^k)^* + \mathfrak{d} (\mathfrak{A}^{k-1})^{-1} \mathfrak{d}^*. \quad (5.6)$$

Here, $*$ denotes the adjoint with respect to the $L^2 \mathfrak{L}^k$ inner product and is the standard matrix transpose in the matrix representation.

In order to show the bound $\kappa(\mathfrak{B}^k \mathfrak{A}^k) \lesssim 1$, we need to verify the conditions in Lemma 5.1 and the results are summarized in the following theorem.

Theorem 5.1. Using \mathfrak{B}^k from (5.6) as a preconditioner for solving the linear system (5.1) leads to a condition number $\kappa(\mathfrak{B}^k \mathfrak{A}^k) \lesssim 1$, where the hidden constant depends only on Ω and shape regularity of the mesh.

Proof. We verify the three conditions of Lemma 5.1:

1. It follows from the properties of Π_h^k and \mathfrak{d} that

$$\|\Pi_h^k \mathbf{a}_h\|_{H\mathfrak{L}^k}^2 = \|\Pi_h^k \mathbf{a}_h\|_{L^2\mathfrak{L}^k}^2 + \|\mathfrak{d}\Pi_h^k \mathbf{a}_h\|_{L^2\mathfrak{L}^{k+1}}^2 \lesssim \|\mathbf{a}_h\|_{H^1\mathfrak{L}^k}^2 + \|\mathfrak{d}\mathbf{a}_h\|_{L^2\mathfrak{L}^{k+1}}^2 \lesssim \|\mathbf{a}_h\|_{H^1\mathfrak{L}^k}^2, \quad (5.7)$$

$$\|\mathfrak{d}\mathbf{f}_h\|_{H\mathfrak{L}^k} = \|\mathfrak{d}\mathbf{f}_h\|_{L^2\mathfrak{L}^k} \leq \|\mathbf{f}_h\|_{H\mathfrak{L}^{k-1}}, \quad (5.8)$$

for any $\mathbf{a}_h \in H_h^1\mathfrak{L}^k$ and $\mathbf{f}_h \in H_h\mathfrak{L}^{k-1}$. This verifies the first condition of Lemma 5.1.

2. Since each element has a finite number of neighbors, there is a small constant $c_s > 0$ such that

$$(\mathbf{q}_h, \mathbf{q}_h)_{\mathfrak{A}^k} = \|\sum_{\mathfrak{e}} q_h^{\mathfrak{e}}\|_{L^2\mathfrak{L}^k}^2 + \|\sum_{\mathfrak{e}} \mathfrak{d}q_h^{\mathfrak{e}}\|_{L^2\mathfrak{L}^{k+1}}^2 \leq c_s^2 \sum_{\mathfrak{e}} (\|q_h^{\mathfrak{e}}\|_{L^2\mathfrak{L}^k}^2 + \|\mathfrak{d}q_h^{\mathfrak{e}}\|_{L^2\mathfrak{L}^{k+1}}^2) = c_s^2 s(\mathbf{q}_h, \mathbf{q}_h), \quad (5.9)$$

which verifies the second condition of Lemma 5.1.

3. Lastly, we can see from Theorem 4.3 that we only need to show the bound on $\|\mathbf{b}_h\|_S$,

$$\begin{aligned} \|\mathbf{b}_h\|_S^2 &= \sum_{\mathfrak{e}} \|b_h^{\mathfrak{e}}\|_{H\mathfrak{L}^k}^2 = \sum_{\mathfrak{e}} (\|b_h^{\mathfrak{e}}\|_{L^2\mathfrak{L}^k}^2 + \|\mathfrak{d}b_h^{\mathfrak{e}}\|_{L^2\mathfrak{L}^{k+1}}^2) \\ &\quad (\text{Inverse inequality}) \lesssim \sum_{\mathfrak{e}} (\|b_h^{\mathfrak{e}}\|_{L^2\mathfrak{L}^k}^2 + \|h^{-1}b_h^{\mathfrak{e}}\|_{L^2\mathfrak{L}^k}^2) \\ &\quad (L^2\text{-stability of the bases}) \lesssim \|\mathbf{b}_h\|_{L^2\mathfrak{L}^k}^2 + \|h^{-1}\mathbf{b}_h\|_{L^2\mathfrak{L}^k}^2 \\ &\quad (\text{Theorem 4.3}) \lesssim \|\mathbf{q}_h\|_{H\mathfrak{L}^k}^2. \end{aligned} \quad (5.10)$$

Therefore, by applying Lemma 5.1, we have that $\kappa(\mathfrak{B}^k\mathfrak{A}^k) \lesssim 1$. \square

We note that it is possible to choose different smoother, such as Gauss-Seidel smoother. In fact, one could use any $s(\cdot, \cdot)$ that is spectral equivalent to $\|h^{-1} \cdot\|_{L^2\mathfrak{L}^k}^2 + \|\cdot\|_{L^2\mathfrak{L}^k}^2$.

Finally, we can integrate the regular decomposition into the preconditioner by utilizing Corollary 4.1 to further expand \mathfrak{B}^k . This will be especially useful in Section 6 when designing a preconditioner for a parameter-dependent saddle point problem in practice. Similarly as before, we set $V = H_h\mathfrak{L}^k$, $W_1 = H_h^1\mathfrak{L}^k$, $W_2 = H_h\mathfrak{L}^{k-1}$ and $W_3 = H_h^1\mathfrak{L}^{k-1}$. The transfer operators are then $\Pi_1 = \Pi_h^k$ restricted to $H_h^1\mathfrak{L}^k$, $\Pi_2 = \mathfrak{d}$ and $\Pi_3 = \mathfrak{d}\Pi_h^{k-1}$ restricted to $H_h^1\mathfrak{L}^{k-1}$. Again, we still use Jacobi smoother for the sake of simplicity here. The preconditioner \mathfrak{B} now has the following form

$$\mathfrak{B}^k = (\mathfrak{S}^k)^{-1} + \Pi_h^k(\mathfrak{A}_{reg}^k)^{-1}(\Pi_h^k)^* + \mathfrak{d}(\mathfrak{S}^{k-1})^{-1}\mathfrak{d}^* + \mathfrak{d}\Pi_h^{k-1}(\mathfrak{A}_{reg}^{k-1})^{-1}(\Pi_h^{k-1})^*\mathfrak{d}^*. \quad (5.11)$$

The next corollary shows the bound $\kappa(\mathfrak{B}^k\mathfrak{A}^k) \lesssim 1$ using \mathfrak{B}^k from (5.11).

Corollary 5.1. *Using \mathfrak{B}^k from (5.11) as a preconditioner for solving the linear system (5.1) leads to a condition number $\kappa(\mathfrak{B}^k\mathfrak{A}^k) \lesssim 1$, where the hidden constant depends only on Ω and shape regularity of the mesh.*

Proof. Since this preconditioner results from the one in (5.6) with further decomposing functions in $H_h\mathfrak{L}^{k-1}$, the conditions in Lemma 5.1 follow from (5.7)–(5.10), which gives the desired result. \square

Remark 5.2. *We emphasize that instead of directly applying inverses of operators \mathfrak{A}_{reg}^k and \mathfrak{A}_{reg}^{k-1} , we can replace them by spectrally equivalent operators, i.e. spectrally equivalent inner products on $H_h^1\mathfrak{L}^k$ and $H_h^1\mathfrak{L}^{k-1}$. Possible choices are multigrid methods and domain decomposition methods.*

Remark 5.3. *For the sake of simplicity, we use model problem (5.3) to derive the mixed-dimensional auxiliary space preconditioner. It is also applicable to the following general problem*

$$\tau(\mathbf{q}_h, \tilde{\mathbf{q}}_h)_{L^2\mathfrak{L}^k} + (\mathfrak{d}\mathbf{q}_h, \mathfrak{d}\tilde{\mathbf{q}}_h)_{L^2\mathfrak{L}^{k+1}} = (\mathbf{f}, \tilde{\mathbf{q}}_h)_{L^2\mathfrak{L}^k} \quad \forall \tilde{\mathbf{q}}_h \in H_h\mathfrak{L}^k.$$

with $\tau > 0$. In fact, such problem appears in the example presented in Section 6 when the mixed-dimensional permeability is a constant.

6 A Practical Example: Flow in Fractured Porous Media

This section presents a practical example in which the theory from the previous sections comes to use. We consider the setting of flow in fractured porous media in which fractures and intersections are modeled as lower-dimensional manifolds. The goal is to solve for a mass-conservative flow field consisting of a flux and a pressure variable. The flux \mathbf{q} is considered as a mixed-dimensional $(n-1)$ -form whereas the pressure distribution \mathbf{p} is represented by a mixed-dimensional n -form [8, 25]. With respect to the diagram (2.5), this model therefore focuses on the bottom two rows.

We consider the natural case of $n = 3$. Then, the flux is defined as a 3-vector in the three-dimensional surroundings, a 2-vector in the two-dimensional fractures, and a scalar in the one-dimensional intersections between fractures. On the other hand, the pressure is defined as a scalar on all manifolds Ω_i with $i \in I$. In this case, instead of using \mathfrak{d} , we denote \mathfrak{D} as the mixed-dimensional differential, which is an analogue of the operator ∇ . Then we represent the complex (2.2) in the same manner as (2.1)

$$H(\mathfrak{D}, \Omega) \xrightarrow{\mathfrak{D}} H(\mathfrak{D} \times, \Omega) \xrightarrow{\mathfrak{D} \times} H(\mathfrak{D} \cdot, \Omega) \xrightarrow{\mathfrak{D} \cdot} L^2(\Omega)$$

The mixed formulation of a fracture flow problem governed by Darcy's law and conservation of mass is then given by: Find $(\mathbf{q}, \mathbf{p}) \in H(\mathfrak{D} \cdot, \Omega) \times L^2(\Omega)$ such that

$$(\mathfrak{K}^{-1} \mathbf{q}, \tilde{\mathbf{q}})_{L^2 \mathfrak{L}^2} - (\mathfrak{D} \cdot \tilde{\mathbf{q}}, \mathbf{p})_{L^2 \mathfrak{L}^3} = 0, \quad \forall \tilde{\mathbf{q}} \in H(\mathfrak{D} \cdot, \Omega), \quad (6.1a)$$

$$(\mathfrak{D} \cdot \mathbf{q}, \tilde{\mathbf{p}})_{L^2 \mathfrak{L}^3} = (\mathfrak{f}, \tilde{\mathbf{p}})_{L^2 \mathfrak{L}^3}, \quad \forall \tilde{\mathbf{p}} \in L^2 \mathfrak{L}^3, \quad (6.1b)$$

where

$$(\mathfrak{K}^{-1} \mathbf{q}, \tilde{\mathbf{q}})_{L^2 \mathfrak{L}^2} := \sum_{d=1}^n \sum_{i \in I^d} (K^{-1} q_i, \tilde{q}_i)_{\Omega_i} + \sum_{j \in I_j^{d-1}} (K_\nu^{-1} \nu_j \cdot q_i, \nu_j \cdot \tilde{q}_i)_{\partial_j \Omega_i} \quad (6.2a)$$

$$(\mathfrak{D} \cdot \mathbf{q}, \tilde{\mathbf{p}})_{L^2 \mathfrak{L}^3} := \sum_{d=0}^n \sum_{i \in I^d} (\iota_i(\mathfrak{D} \cdot \mathbf{q}), \tilde{\mathbf{p}}_i)_{\Omega_i}. \quad (6.2b)$$

Here, \mathfrak{f} is a given source term. \mathfrak{K} is the mixed-dimensional permeability tensor given by a tangential and a normal component, denoted by K and K_ν , respectively.

6.1 Discrete Problem

For the discretization, we follow Section 4 and choose the finite element spaces given by the final two rows in diagram (4.4). Note that this corresponds to the mixed finite element scheme presented and analyzed in [8]. In short, we choose $H_h \mathfrak{L}^2 \times H_h \mathfrak{L}^3$ as in diagram (4.4) and consider the discrete problem: Find $(\mathbf{q}_h, \mathbf{p}_h) \in H_h \mathfrak{L}^2 \times H_h \mathfrak{L}^3$ such that

$$(\mathfrak{K}^{-1} \mathbf{q}_h, \tilde{\mathbf{q}}_h)_{L^2 \mathfrak{L}^2} - (\mathfrak{D} \cdot \tilde{\mathbf{q}}_h, \mathbf{p}_h)_{L^2 \mathfrak{L}^3} = 0, \quad \forall \tilde{\mathbf{q}}_h \in H_h \mathfrak{L}^2, \quad (6.3a)$$

$$(\mathfrak{D} \cdot \mathbf{q}_h, \tilde{\mathbf{p}}_h)_{L^2 \mathfrak{L}^3} = (\mathfrak{f}, \tilde{\mathbf{p}}_h)_{L^2 \mathfrak{L}^3}, \quad \forall \tilde{\mathbf{p}}_h \in H_h \mathfrak{L}^3. \quad (6.3b)$$

We briefly verify that problem (6.3) is well-posed. For that, we define the weighted norms

$$\|\mathbf{q}_h\|_{H_\alpha \mathfrak{L}^2}^2 := \|\mathfrak{K}^{-\frac{1}{2}} \mathbf{q}_h\|_{L^2 \mathfrak{L}^2}^2 + \alpha \|\mathfrak{D} \cdot \mathbf{q}_h\|_{L^2 \mathfrak{L}^3}^2, \quad (6.4a)$$

$$\|\mathbf{p}_h\|_{H_\alpha \mathfrak{L}^3}^2 := \alpha^{-1} \|\mathbf{p}_h\|_{L^2 \mathfrak{L}^3}^2. \quad (6.4b)$$

Here, the scalar α is chosen such that $\alpha \geq \mathfrak{K}_{\min}^{-1}$ with $\mathfrak{K}_{\min} > 0$ being the minimal eigenvalue of \mathfrak{K} . In turn, we have

$$\|\mathfrak{K}^{-\frac{1}{2}} \mathbf{q}_h\|_{L^2 \mathfrak{L}^2}^2 \leq \alpha \|\mathbf{q}_h\|_{L^2 \mathfrak{L}^2}^2, \quad \forall \mathbf{q}_h \in H_h \mathfrak{L}^2. \quad (6.5)$$

A key result in the analysis of this problem is that the pair of finite element spaces $H_h \mathfrak{L}^2 \times H_h \mathfrak{L}^3$ satisfies the following inf-sup condition with respect to the weighted norms (6.4).

Lemma 6.1. *There exists a constant $\gamma_B > 0$ independent of the discretization parameter h and the physical parameter \mathfrak{K} such that*

$$\inf_{\mathbf{p}_h \in H_h \mathfrak{L}^3} \sup_{\mathbf{q}_h \in H_h \mathfrak{L}^2} \frac{-(\mathfrak{D} \cdot \mathbf{q}_h, \mathbf{p}_h)_{L^2 \mathfrak{L}^3}}{\|\mathbf{q}_h\|_{H_\alpha \mathfrak{L}^2} \|\mathbf{p}_h\|_{H_\alpha \mathfrak{L}^3}} \geq \gamma_B. \quad (6.6)$$

Proof. For any given $\mathbf{p}_h \in H_h \mathfrak{L}^3$, according to the inf-sup condition proven in [8] (Lemma 3.2), there exists a $\mathbf{q}_h \in H_h \mathfrak{L}^2$ such that

$$\begin{aligned} -(\mathfrak{D} \cdot \mathbf{q}_h, \mathbf{p}_h)_{L^2 \mathfrak{L}^3} &= \|\mathbf{p}_h\|_{L^2 \mathfrak{L}^3}^2, \\ \|\mathfrak{K}^{-\frac{1}{2}} \mathbf{q}_h\|_{L^2 \mathfrak{L}^2}^2 + \|\mathfrak{D} \cdot \mathbf{q}_h\|_{L^2 \mathfrak{L}^3}^2 &\lesssim \|\mathbf{p}_h\|_{L^2 \mathfrak{L}^3}^2. \end{aligned}$$

Using these properties and (6.5), it follows that

$$\begin{aligned} -(\mathfrak{D} \cdot \mathbf{q}_h, \mathbf{p}_h)_{L^2 \mathfrak{L}^3} &= \|\mathbf{p}_h\|_{L^2 \mathfrak{L}^3}^2 \\ &= \left(\alpha^{-\frac{1}{2}} \|\mathbf{p}_h\|_{L^2 \mathfrak{L}^3} \right) \left(\alpha^{\frac{1}{2}} \|\mathbf{p}_h\|_{L^2 \mathfrak{L}^3} \right) \\ &\gtrsim \|\mathbf{p}_h\|_{H_\alpha \mathfrak{L}^3} \left(\alpha \|\mathbf{q}_h\|_{L^2 \mathfrak{L}^2}^2 + \alpha \|\mathfrak{D} \cdot \mathbf{q}_h\|_{L^2 \mathfrak{L}^3}^2 \right)^{\frac{1}{2}} \\ &\geq \|\mathbf{p}_h\|_{H_\alpha \mathfrak{L}^3} \|\mathbf{q}_h\|_{H_\alpha \mathfrak{L}^2}. \end{aligned}$$

This completes the proof. \square

Based on Lemma 6.1, we can show the well-posedness of problem (6.3) by introducing the following spaces and weighted norms. Let $\mathfrak{X} := H_h \mathfrak{L}^2 \times H_h \mathfrak{L}^3$ and \mathfrak{X}' be the corresponding dual space. Let the energy norm on \mathfrak{X} be given by

$$\|\mathfrak{r}\|_{\mathfrak{X}}^2 = \|(\mathbf{q}_h, \mathbf{p}_h)\|_{\mathfrak{X}}^2 = \|\mathbf{q}_h\|_{H_\alpha \mathfrak{L}^2}^2 + \|\mathbf{p}_h\|_{H_\alpha \mathfrak{L}^3}^2, \quad (6.7)$$

which is induced by the inner product $(\cdot, \cdot)_{\mathfrak{X}}$, i.e. $(\mathfrak{r}, \mathfrak{r})_{\mathfrak{X}} = \|\mathfrak{r}\|_{\mathfrak{X}}^2$. In addition, let us introduce the following composite bilinear form

$$\mathcal{L}(\mathfrak{r}, \mathfrak{r}) := (\mathfrak{K}^{-1} \mathbf{q}_h, \tilde{\mathbf{q}}_h)_{L^2 \mathfrak{L}^2} - (\mathfrak{D} \cdot \tilde{\mathbf{q}}_h, \mathbf{p}_h)_{L^2 \mathfrak{L}^3} + (\mathfrak{D} \cdot \mathbf{q}_h, \tilde{\mathbf{p}}_h)_{L^2 \mathfrak{L}^3}, \quad (6.8)$$

for $\mathfrak{r} = (\mathbf{q}_h, \mathbf{p}_h)$ and $\mathfrak{r} = (\tilde{\mathbf{q}}_h, \tilde{\mathbf{p}}_h)$. Now we can show the problem (6.3) is well-posed, as presented in the following theorem.

Theorem 6.1. *There exist constants $\beta, \gamma > 0$ independent of discretization parameter h and physical parameter \mathfrak{K} such that*

$$\inf_{\mathfrak{r} \in \mathfrak{X}} \sup_{\mathfrak{r} \in \mathfrak{X}} \frac{\mathcal{L}(\mathfrak{r}, \mathfrak{r})}{\|\mathfrak{r}\|_{\mathfrak{X}} \|\mathfrak{r}\|_{\mathfrak{X}}} \geq \gamma \quad \text{and} \quad |\mathcal{L}(\mathfrak{r}, \mathfrak{r})| \leq \beta \|\mathfrak{r}\|_{\mathfrak{X}} \|\mathfrak{r}\|_{\mathfrak{X}}, \quad \forall \mathfrak{r}, \mathfrak{r} \in \mathfrak{X}. \quad (6.9)$$

Proof. Let $\mathfrak{r} = (\mathbf{q}_h, \mathbf{p}_h) \in \mathfrak{X}$. Due to the inf-sup condition in Lemma 6.1, there exists $\mathbf{r}_h \in H_h \mathfrak{L}^2$ for this given \mathbf{p}_h such that

$$-(\mathfrak{D} \cdot \mathbf{r}_h, \mathbf{p}_h)_{L^2 \mathfrak{L}^3} \geq \gamma_B \|\mathbf{p}_h\|_{H_\alpha \mathfrak{L}^3}^2, \quad (6.10a)$$

$$\|\mathbf{r}_h\|_{H_\alpha \mathfrak{L}^2}^2 = \|\mathbf{p}_h\|_{H_\alpha \mathfrak{L}^3}^2. \quad (6.10b)$$

Then, choose $\mathfrak{r} = (\tilde{\mathbf{q}}_h, \tilde{\mathbf{p}}_h)$ such that $\tilde{\mathbf{q}}_h = \mathbf{q}_h + \gamma_B \mathbf{r}_h$ and $\tilde{\mathbf{p}}_h = \mathbf{p}_h + \alpha \mathfrak{D} \cdot \mathbf{q}_h$, and use (6.10) together with Cauchy-Schwarz inequality, we have

$$\begin{aligned} \mathcal{L}(\mathfrak{r}, \mathfrak{r}) &= (\mathfrak{K}^{-1} \mathbf{q}_h, \mathbf{q}_h + \gamma_B \mathbf{r}_h)_{L^2 \mathfrak{L}^2} - (\mathfrak{D} \cdot (\mathbf{q}_h + \gamma_B \mathbf{r}_h), \mathbf{p}_h)_{L^2 \mathfrak{L}^3} + (\mathfrak{D} \cdot \mathbf{q}_h, \mathbf{p}_h + \alpha \mathfrak{D} \cdot \mathbf{q}_h)_{L^2 \mathfrak{L}^3} \\ &= \|\mathfrak{K}^{-\frac{1}{2}} \mathbf{q}_h\|_{L^2 \mathfrak{L}^2}^2 + \gamma_B (\mathfrak{K}^{-1} \mathbf{q}_h, \mathbf{r}_h)_{L^2 \mathfrak{L}^2} - \gamma_B (\mathfrak{D} \cdot \mathbf{r}_h, \mathbf{p}_h)_{L^2 \mathfrak{L}^3} + \alpha \|\mathfrak{D} \cdot \mathbf{q}_h\|_{L^2 \mathfrak{L}^3}^2 \\ &\geq \|\mathfrak{K}^{-\frac{1}{2}} \mathbf{q}_h\|_{L^2 \mathfrak{L}^2}^2 - \frac{1}{2} \|\mathfrak{K}^{-\frac{1}{2}} \mathbf{q}_h\|_{L^2 \mathfrak{L}^2}^2 - \frac{\gamma_B^2}{2} \|\mathfrak{K}^{-\frac{1}{2}} \mathbf{r}_h\|_{L^2 \mathfrak{L}^2}^2 + \gamma_B^2 \|\mathbf{p}_h\|_{H_\alpha \mathfrak{L}^3}^2 + \alpha \|\mathfrak{D} \cdot \mathbf{q}_h\|_{L^2 \mathfrak{L}^3}^2 \\ &\geq \frac{1}{2} \|\mathfrak{K}^{-\frac{1}{2}} \mathbf{q}_h\|_{L^2 \mathfrak{L}^2}^2 - \frac{\gamma_B^2}{2} \|\mathbf{r}_h\|_{H_\alpha \mathfrak{L}^2}^2 + \gamma_B^2 \|\mathbf{p}_h\|_{H_\alpha \mathfrak{L}^3}^2 + \alpha \|\mathfrak{D} \cdot \mathbf{q}_h\|_{L^2 \mathfrak{L}^3}^2 \\ &= \frac{1}{2} \|\mathfrak{K}^{-\frac{1}{2}} \mathbf{q}_h\|_{L^2 \mathfrak{L}^2}^2 + \frac{\gamma_B^2}{2} \|\mathbf{p}_h\|_{H_\alpha \mathfrak{L}^3}^2 + \alpha \|\mathfrak{D} \cdot \mathbf{q}_h\|_{L^2 \mathfrak{L}^3}^2 \\ &\geq \frac{1}{2} \min\{1, \gamma_B^2\} (\|\mathbf{q}_h\|_{H_\alpha \mathfrak{L}^2}^2 + \|\mathbf{p}_h\|_{H_\alpha \mathfrak{L}^3}^2) \\ &= \frac{1}{2} \min\{1, \gamma_B^2\} \|\mathfrak{r}\|_{\mathfrak{X}}^2. \end{aligned}$$

On the other hand, using continuity of the norms and Cauchy-Schwarz inequality, it is straightforward to verify that $\|\mathfrak{q}\|_{\mathfrak{X}}^2 \leq \frac{\sqrt{2}}{2} \|\mathfrak{x}\|_{\mathfrak{X}}^2$, and that gives the first condition in (6.9). The same arguments can be applied to get the second condition on $\mathcal{L}(\cdot, \cdot)$ in (6.9), which concludes the proof. \square

6.2 Block Preconditioners based on Auxiliary Space Preconditioning

Let $\langle \cdot, \cdot \rangle$ denote the duality pairing between a function space and its dual. The discrete system (6.3) can be represented by the following block operator form

$$\mathcal{A} \begin{pmatrix} \mathbf{q}_h \\ \mathbf{p}_h \end{pmatrix} = \begin{pmatrix} 0 \\ \mathbf{f} \end{pmatrix} \quad \text{with} \quad \mathcal{A} := \begin{pmatrix} A_{\mathbf{q}} & -B^T \\ B & 0 \end{pmatrix}, \quad (6.11)$$

where $\langle A_{\mathbf{q}} \mathbf{q}_h, \tilde{\mathbf{q}}_h \rangle := (\mathfrak{K}^{-1} \mathbf{q}_h, \tilde{\mathbf{q}}_h)_{L^2 \mathfrak{L}^2}$ and $\langle B \mathbf{q}_h, \tilde{\mathbf{p}}_h \rangle := (\mathfrak{D} \cdot \mathbf{q}_h, \tilde{\mathbf{p}}_h)_{L^2 \mathfrak{L}^3}$.

According to Theorem 6.1, \mathcal{A} is an isomorphism with respect to the weighted energy norm (6.7). Following the standard framework [23], the canonical block preconditioner for solving the linear system (6.11) is the Riesz operator $\mathcal{B} : \mathfrak{X}' \mapsto \mathfrak{X}$ corresponding to the inner product $(\cdot, \cdot)_{\mathfrak{X}}$, i.e.,

$$(\mathcal{B} \mathbf{f}, \mathbf{r})_{\mathfrak{X}} = \langle \mathbf{f}, \mathbf{r} \rangle, \quad \forall \mathbf{f} \in \mathfrak{X}', \mathbf{r} \in \mathfrak{X}.$$

It follows from Theorem 6.1 that,

$$\kappa(\mathcal{B}\mathcal{A}) = \|\mathcal{B}\mathcal{A}\|_{\mathcal{L}(\mathfrak{X}, \mathfrak{X})} \|(\mathcal{B}\mathcal{A})^{-1}\|_{\mathcal{L}(\mathfrak{X}, \mathfrak{X})} \leq \frac{\beta}{\gamma}. \quad (6.12)$$

If β and γ are independent of the discretization and physical parameters, then \mathcal{B} is a robust preconditioner for linear system (6.11). Based on the definition of the weighted energy norm (6.7), the preconditioner \mathcal{B} takes the following block diagonal form

$$\mathcal{B} = \begin{pmatrix} A_{\mathbf{q}} + \alpha B^T B & 0 \\ 0 & \alpha^{-1} A_{\mathbf{p}} \end{pmatrix}^{-1} = \begin{pmatrix} (A_{\mathbf{q}} + \alpha B^T B)^{-1} & 0 \\ 0 & \alpha A_{\mathbf{p}}^{-1} \end{pmatrix}, \quad (6.13)$$

where $\langle A_{\mathbf{p}} \mathbf{p}_h, \mathbf{p}_h \rangle := (\mathbf{p}_h, \mathbf{p}_h)_{L^2 \mathfrak{L}^n}$.

Remark 6.1. The top block $(A_{\mathbf{q}} + \alpha B^T B)^{-1}$ in the preconditioner \mathcal{B} corresponds to applying the augmented Lagrangian method to a parameter-dependent problem (6.11). The method is well-known and used in literature [13, 21, 28] for general elliptic problems since it effectively handles the difficulties in convergence of general iterative methods, such as the physical parameter \mathfrak{K} affecting the condition number of the linear system.

In practice, directly inverting the diagonal blocks in (6.13) might not be feasible. To overcome this difficult, we replace the diagonal blocks by their spectrally equivalent approximation and propose the following block diagonal preconditioner,

$$\mathcal{M}_D = \begin{pmatrix} M_{\mathbf{q}} & 0 \\ 0 & M_{\mathbf{p}} \end{pmatrix},$$

where

$$\begin{aligned} c_{1,\mathbf{q}} \langle M_{\mathbf{q}} \mathbf{q}_h, \mathbf{q}_h \rangle &\leq \langle (A_{\mathbf{q}} + \alpha B^T B)^{-1} \mathbf{q}_h, \mathbf{q}_h \rangle \leq c_{2,\mathbf{q}} \langle M_{\mathbf{q}} \mathbf{q}_h, \mathbf{q}_h \rangle, \\ c_{1,\mathbf{p}} \langle M_{\mathbf{p}} \mathbf{p}_h, \mathbf{p}_h \rangle &\leq \langle \alpha A_{\mathbf{p}}^{-1} \mathbf{p}_h, \mathbf{p}_h \rangle \leq c_{2,\mathbf{p}} \langle M_{\mathbf{p}} \mathbf{p}_h, \mathbf{p}_h \rangle, \end{aligned}$$

where $c_{1,\mathbf{q}}$, $c_{1,\mathbf{p}}$, $c_{2,\mathbf{q}}$, and $c_{2,\mathbf{p}}$ are positive constants independent of discretization and physical parameters. Following [9, 23] and using Theorem 6.1 and (6.12), the condition number of $\mathcal{M}_D \mathcal{A}$ can be directly estimated as

$$\kappa(\mathcal{M}_D \mathcal{A}) \leq \frac{\beta c_2}{\gamma c_1},$$

for $c_2 = \max\{c_{2,\mathbf{q}}, c_{2,\mathbf{p}}\}$ and $c_1 = \min\{c_{1,\mathbf{q}}, c_{1,\mathbf{p}}\}$. Again, if β , γ , c_1 , and c_2 are independent of the discretization and physical parameters, then \mathcal{M}_D is a robust preconditioner as well.

Now we discuss our choices of M_q and M_p . We start with M_p . Due to the fact that the choice of finite element space for the pressure variable is piecewise constant, it follows that the corresponding mass matrix is diagonal and thus, easily invertible. Therefore, we take $M_p = \alpha A_p^{-1}$ and, naturally, $c_{1,p} = c_{2,p} = 1$.

Regarding M_q , since the first block $A_q + \alpha B^T B$ corresponds to the problem

$$(\mathcal{K}^{-1} \mathbf{q}_h, \tilde{\mathbf{q}}_h)_{L^2 \mathcal{L}^2} + \alpha (\mathcal{D} \cdot \mathbf{q}_h, \mathcal{D} \cdot \tilde{\mathbf{q}}_h)_{L^2 \mathcal{L}^3}. \quad (6.14)$$

It is quite challenging to solve it using traditional methods due to the large kernel of the operator $\mathcal{D} \cdot$. Therefore, we propose to use the mixed-dimensional auxiliary space preconditioner (5.11), derived in Section 5.2. The form (6.14) can be viewed as a special case of the mixed dimensional problem (5.1) when $n = 3$, $k = 2$, and certain coefficients are added. Directly apply the auxiliary space preconditioner (5.11), we have

$$\mathfrak{B}^2 = (\mathfrak{S}^2)^{-1} + \Pi_h^2 (\mathfrak{A}_{reg}^2)^{-1} (\Pi_h^2)^* + (\mathcal{D} \times) (\mathfrak{S}^1)^{-1} (\mathcal{D} \times)^* + (\mathcal{D} \times) (\Pi_h^1) (\mathfrak{A}_{reg}^1)^{-1} (\Pi_h^1)^* (\mathcal{D} \times)^*.$$

The smoothers \mathfrak{S}^2 and \mathfrak{S}^1 are chosen to satisfy the second condition in Lemma 5.1. In our implementation, we use symmetric Gauss-Seidel smoothers for both cases. Since the regular space $H_h^1 \mathcal{L}^2$ is given by d_i -tuples of linear Lagrange elements on each $\Omega_{i,h}$ with $i \in I$ and $d_i \geq 1$ and $H_h^1 \mathcal{L}^1$ is defined for $i \in I^3$ (respectively I^2) as a 3-vector field (respectively scalar field) of linear Lagrange elements on $\Omega_{i,h}$, \mathfrak{A}_{reg}^2 and \mathfrak{A}_{reg}^1 represent the (weighted) inner products on these spaces from (3.6). Moreover, it is often advantageous to further substitute spectrally equivalent operators for $(\mathfrak{A}_{reg}^k)^{-1}$, $k = 2, 1$, denoted by \mathfrak{B}_{reg}^k , then the overall auxiliary space preconditioner for solving (6.14) is

$$\mathfrak{B}_q := (\mathfrak{S}^2)^{-1} + \Pi_h^2 \mathfrak{B}_{reg}^2 (\Pi_h^2)^* + (\mathcal{D} \times) (\mathfrak{S}^1)^{-1} (\mathcal{D} \times)^* + (\mathcal{D} \times) (\Pi_h^1) \mathfrak{B}_{reg}^1 (\Pi_h^1)^* (\mathcal{D} \times)^*. \quad (6.15)$$

and our choice of M_q is defined as solving (6.14) by Generalize Minimal Residual (GMRES) method with \mathfrak{B}_q as the preconditioner. In our implementation, \mathfrak{B}_{reg}^k , $k = 2, 1$, are defined by one W-cycle unsmoothed aggregation algebraic multigrid method. A theoretical study of their spectrally equivalence properties and thorough comparison of the different available choices is outside the scope of this work and are subjects of our future work.

Lastly, we also consider two block triangular preconditioners

$$\mathcal{M}_L = \begin{pmatrix} M_q^{-1} & 0 \\ -B & M_p^{-1} \end{pmatrix}^{-1} \quad \text{and} \quad \mathcal{M}_U = \begin{pmatrix} M_q^{-1} & B^T \\ 0 & M_p^{-1} \end{pmatrix}^{-1},$$

where \mathcal{M}_L serves as a uniform left and \mathcal{M}_U as a uniform right preconditioner for solving (6.11). It can be proven that \mathcal{M}_L and \mathcal{M}_U are so-called field-of-value (FoV) equivalent preconditioners based on the well-posedness conditions (6.9) and proper inner product induced by \mathcal{M}_D . We refer the reader to [1, 2, 9, 22] for a more detailed theoretical analysis on these preconditioners and restrict our focus on their numerical performances in the next section.

7 Numerical Examples

In this section, we propose several numerical tests to confirm the theory derived in previous sections. These tests are designed to emphasize common challenges related to mixed-dimensional problems, such as the geometric complexity and parameter heterogeneity. Also, the problems represent simplified mathematical models of common applications, in this case the model of flow in fractured porous media introduced in Section 6.

In each example, we generate separate simplicial grids on rock and fracture subdomains which combined produce mixed-dimensional geometry Ω . For the sake of simplicity, we assume that Ω is of rectangular type and all the adjacent grids are matching. We want to point out that the analysis presented in this paper allows more flexibility in the geometrical structure.

To solve the system (6.11), we use a Flexible Generalized Minimal Residual (FGMRES) method as an *outer* iterative solver and set the tolerance to be the relative residual less than 10^{-6} . We precondition the outer FGMRES solver with the block preconditioners designed in Section 6.2, i.e., the block diagonal preconditioner \mathcal{M}_D and the block triangular preconditioners \mathcal{M}_L and \mathcal{M}_U . As mentioned, the pressure block $\alpha^{-1}A_p$ is represented as a diagonal matrix using piecewise constant finite elements, thus the inverse is given straightforwardly. On the other hand, the flux block $A_q + \alpha B^T B$ is approximated by M_q which is defined by GMRES method preconditioned by the mixed-dimensional auxiliary space preconditioner \mathfrak{B}_q (6.15). We refer this as the inner solver with a relative residual tolerance set to 10^{-3} . To define \mathfrak{B}_q , we use symmetric Gauss-Seidel method as smoothers $(\mathfrak{S}^2)^{-1}$ and $(\mathfrak{S}^1)^{-1}$, and one application of W-cycle unsmoothed aggregation Algebraic Multigrid method (UA-AMG) as \mathfrak{B}_{reg}^2 and \mathfrak{B}_{reg}^1 .

For obtaining the mixed-dimensional geometry and discretization, we use the PorePy library [18], an open-source simulation tool for fractured and deformable porous media written in Python. The solving methods and preconditioners are implemented in HAZMATH library [3], a finite element solver library written in C. The following numerical examples are performed on a workstation with an 8-core 3GHz Intel Xeon "Sandy Bridge" CPU and 256 GB of RAM.

7.1 Example: Three-dimensional Regular network

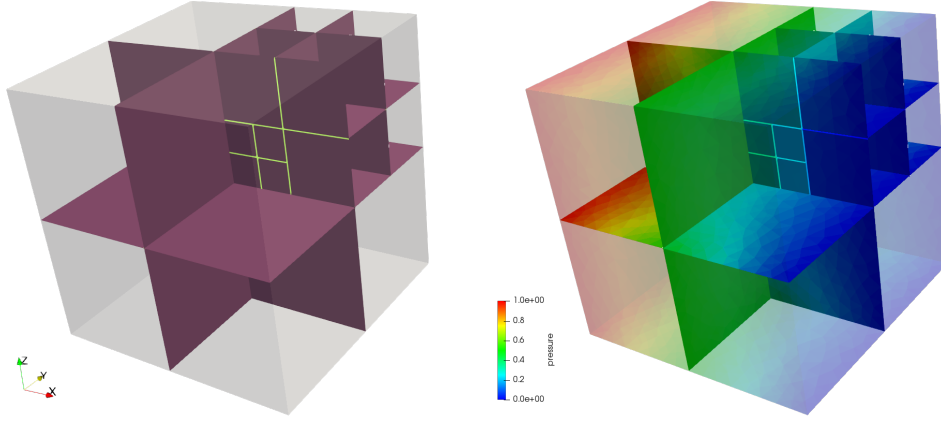


Figure 2: (Left) The three-dimensional unit cube domain in Example 7.1 is decomposed by 9 fracture planes, 9 intersection lines and 1 intersection point. (Right) Pressure solution is presented for the case of a homogeneous permeability tensor $\mathfrak{K} = \mathbf{I}$ and a mesh size $h = 1/16$.

This example considers simulations of a 3D problem taken from the benchmark study [6], that is, a three-dimensional Geiger fracture network. The rock domain is a unit cube intersected with a fracture network that consists of nine intersecting planes. The physical parameters are set as following: we take the fracture aperture to be 10^{-2} and the mixed-dimensional permeability tensor is homogeneous $\mathfrak{K} = \mathbf{I}$. Within \mathfrak{K} , we take into account that due to the reduced model scaling, the tangential K and the normal component K_ν represent the effective values of the permeability field. See [6] for more details. Furthermore, in the heterogeneous case, we consider splitting the tangential permeability into the rock matrix permeability K_m and fracture permeability K_f to allow for different flow patterns within the fracture network, either conducting or blocking the flow in the tangential direction. Also, we consider higher or lower normal permeability K_ν that conducts or blocks the flow over the interface between the rock and the fractures. At the boundary, we impose pressure boundary conditions with unitary pressure drop from $x = 0$ to $x = 1$ boundary planes. The boundary conditions are applied to both the rock matrix and the fracture network. A graphical illustration of the geometry and the numerical solution is given in Figure 2.

Our goal is to investigate the robustness of the block preconditioners in Section 5.2. with respect to discretization parameter h and physical parameter \mathfrak{K} . We also vary the scaling parameter α to

study the influence on the convergence rate of the solver and how it changes with the heterogeneous permeability field. We compute and compare number of iterations of the outer and inner solver, as well as the elapsed process (CPU) time of the solver with regards to the number of degrees of freedom.

| h | N_{dof} | \mathcal{M}_D | | | \mathcal{M}_L | | | \mathcal{M}_U | | |
|------|-----------|-----------------|-----------|-------|-----------------|-----------|-------|-----------------|-----------|-------|
| | | N_{it} | T_{cpu} | rate | N_{it} | T_{cpu} | rate | N_{it} | T_{cpu} | rate |
| 1/4 | 7173 | 12 (5) | 0.331 | – | 20 (5) | 0.402 | – | 20 (4) | 0.351 | – |
| 1/8 | 17172 | 11 (6) | 0.580 | 0.643 | 19 (5) | 0.617 | 0.492 | 19 (5) | 0.553 | 0.523 |
| 1/16 | 89731 | 11 (6) | 3.229 | 1.039 | 19 (7) | 4.265 | 1.169 | 20 (5) | 3.716 | 1.152 |
| 1/32 | 518291 | 11 (8) | 31.569 | 1.300 | 17 (8) | 39.499 | 1.269 | 18 (7) | 37.431 | 1.317 |
| 1/64 | 3375415 | 11 (11) | 356.098 | 1.293 | 17 (11) | 482.206 | 1.335 | 18 (9) | 436.261 | 1.311 |

Table 1: Performance of the outer FGMRES solver using preconditioners \mathcal{M}_D , \mathcal{M}_L and \mathcal{M}_U in Section 7.1 with regards to mesh refinement. For each preconditioner, we report number of outer (average inner) iterations N_{it} needed to reach the prescribed tolerance and overall elapsed CPU time T_{cpu} . Last column presents the exponential rate of T_{cpu} of outer solver with regards to total degrees of freedom N_{dof} . The permeability tensor is homogeneous and set to $\mathfrak{K} = \mathbf{I}$ and the scaling parameter is set to $\alpha = 1$.

The following tables consider the homogeneous permeability case with $\mathfrak{K} = \mathbf{I}$ and $\alpha = 1$. In Table 1, we present the results to study the robustness of the preconditioners with respect to the mesh refinement, where each row stands for a mesh twice finer than the previous one. For each preconditioner \mathcal{M}_D , \mathcal{M}_L and \mathcal{M}_U we give the number of iterations N_{it} of the outer FGMRES solver followed by average number of iterations of the inner GMRES solver in brackets, as well as the CPU time T_{cpu} of the solving process and the exponential rate of the CPU time with regards to the number of degrees of freedom N_{dof} . We clearly see that all preconditioners show that the number of iterations of the outer solver stays stable when refining the mesh, while there is a slight increase of iterations in the inner solver, which is due to our choice of \mathfrak{B}_{reg}^2 and \mathfrak{B}_{reg}^1 . Therefore, we can conclude that preconditioners are robust with regards to the mesh size h , but it suggests a different choice of the inner solver. As mentioned before, the inner solver performance depends on the choices of the spectrally equivalent approximations \mathfrak{B}_{reg}^2 and \mathfrak{B}_{reg}^1 of operators $(\mathfrak{A}_{reg}^2)^{-1}$ and $(\mathfrak{A}_{reg}^1)^{-1}$, respectively. These operators are represented in the nodal basis giving a Laplacian-type structure and thus, we have chosen UA-AMG as the approximation method. However, a further analysis that this UA-AMG approximation is actually spectrally equivalent is needed. Although the operators \mathfrak{A}_{reg}^2 and \mathfrak{A}_{reg}^1 act as a vector-Laplacian on each subdomain, they are still mixed-dimensional, and the off-diagonal coupling between the subdomains is still present which possibly diminishes the preferable structure for AMG methods. Moreover, this suboptimal behavior can be seen in the exponential rates of the CPU time T_{cpu} of the total solving process with regards to the total number of degrees of freedom N_{dof} . We expect T_{cpu} to scale as $\mathcal{O}(N_{dof})$, giving a rate ≈ 1 , but all preconditioners show rate closer to 1.3. This is also visible in Figure 3 where the increase in T_{cpu} fairly follows, but does not match the linear rate line. Even with a suboptimal process time performance, we still believe the preconditioners to be working well on the given problem setup, and consider the investigating proper spectrally equivalent approximations of operators $(\mathfrak{A}_{reg}^2)^{-1}$ and $(\mathfrak{A}_{reg}^1)^{-1}$ in future research.

While still taking the permeability tensor to be homogeneous and unitary, we set the mesh size to $h = 1/32$ and study the performance of the preconditioners with a range of values of the parameter α . Although the theory suggests taking any $\alpha \geq \mathfrak{K}_{min}^{-1}$, we consider instead $\alpha \geq \max\{1, \mathfrak{K}_{min}^{-1}\}$ to achieve reasonable convergence of the underlying augmented Lagrangian method. Table 2 shows the results of the overall outer (and average inner) number of iterations for both diagonal and triangular preconditioners. As expected, the performance of block preconditioners improves with higher values of α since, according to the theory of the augmented Lagrangian method [13], the iterative method should converge faster in those cases. On the other hand, increasing α gives more weight on the mixed-dimensional divergence part of the inner product (6.14), which makes the problem at each inner iteration nearly singular [21, 28]. This may slightly deteriorate the performance of the inner GMRES method, that mostly affects the UA-AMG method

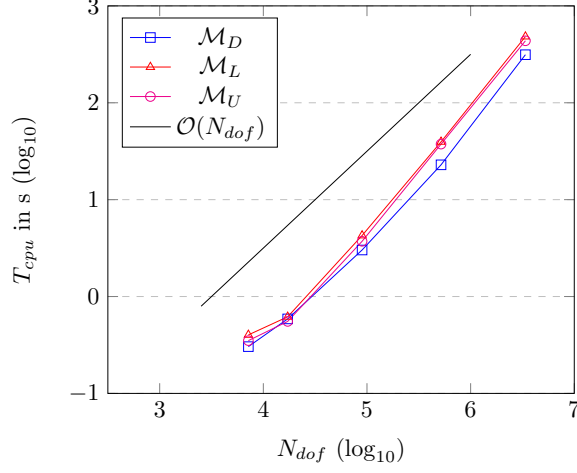


Figure 3: CPU time T_{cpu} of FGMRES solver with block preconditioners compared to total number of degrees of freedom N_{dof} of the linear system in Section 7.1. The values of T_{cpu} and N_{dof} are taken from Table 1. We mark $\mathcal{O}(N_{dof})$ complexity with a black continuous line.

| α | \mathcal{M}_D | \mathcal{M}_L | \mathcal{M}_U |
|----------|-----------------|-----------------|-----------------|
| 10^0 | 11 (8) | 17 (8) | 18 (7) |
| 10^1 | 6 (9) | 9 (9) | 10 (8) |
| 10^2 | 5 (10) | 7 (10) | 7 (8) |
| 10^3 | 4 (12) | 5 (11) | 7 (9) |
| 10^4 | 4 (13) | 4 (13) | 6 (10) |

Table 2: Performance of the outer FGMRES solver using preconditioners \mathcal{M}_D , \mathcal{M}_L and \mathcal{M}_U in Section 7.1 with regards to varying the scaling parameter α . For each preconditioner, we report number of outer (average inner) iterations needed to reach the prescribed tolerance. The permeability tensor is homogeneous and set to $\mathfrak{K} = \mathbf{I}$ and mesh size is set to $h = 1/32$.

within it. Nevertheless, we find a good balance to performance of both the outer and inner solver to be around $\alpha = \max\{1, 100\mathfrak{K}_{min}^{-1}\}$. This can be observed in the study on the heterogeneous permeability field in Table 3. Here, we set the tangential rock component of the permeability to be $K_m = \mathbf{I}$, while the tangential fracture component K_f and the normal fracture component K_ν in conjunction assume different values, from low to high permeable case. The results show similar behavior as in Table 2: we get a lower number of outer iterations for $\alpha \gg \max\{1, \mathfrak{K}_{min}^{-1}\}$, but in turn the inner number of iteration increases. Therefore, in this example, we can conclude that taking $\alpha = \max\{1, 100\mathfrak{K}_{min}^{-1}\}$ gives the optimal performance of the preconditioned iterative method.

| α | $K_f = K_\nu$ | | | | |
|----------|---------------|-----------|--------|--------|--------|
| | 10^{-4} | 10^{-2} | 10^0 | 10^2 | 10^4 |
| 10^0 | – | – | 11 (5) | 5 (5) | 5 (13) |
| 10^2 | – | 11 (5) | 5 (6) | 4 (9) | 4 (14) |
| 10^4 | 11 (5) | 5 (6) | 4 (15) | 4 (22) | 4 (41) |

Table 3: Performance of the outer FGMRES solver using preconditioners \mathcal{M}_D , \mathcal{M}_L and \mathcal{M}_U in Section 7.1 with regards to varying the scaling parameter α and the lowest eigenvalue of the permeability tensor \mathfrak{K}_{min} . The variations in the eigenvalue spectrum come from the heterogeneity of the fractured porous medium: the tangential rock component of the permeability is $K_m = \mathbf{I}$, while we vary the tangential fracture component K_f and the normal fracture component K_ν . For each preconditioner, we report number of outer (average inner) iterations needed to reach the prescribed tolerance. The mesh size is set to $h = 1/16$.

7.2 Example: Two-dimensional Complex Network

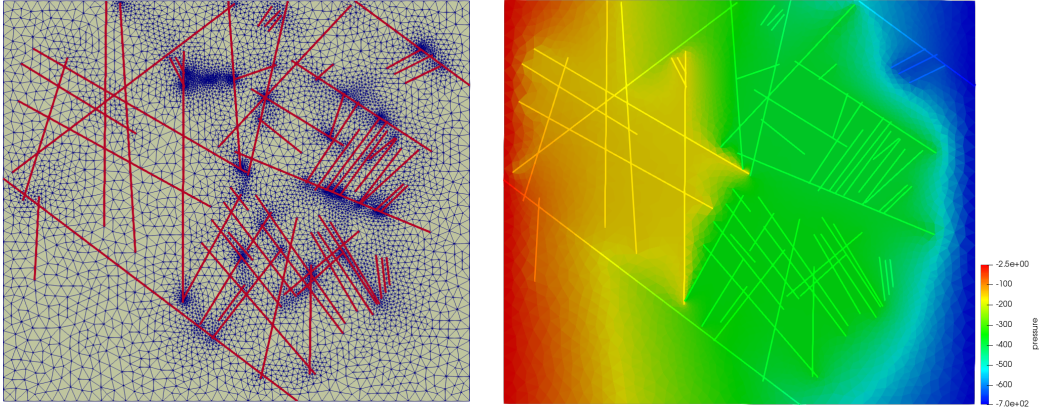


Figure 4: (Left) Graphical representation of the two-dimensional domain and fracture network geometry of Example 7.2. (Right) Pressure solution profile.

We provide another example, chosen from the benchmark study [12], which contains a fracture network from an interpreted outcrop in the Sotra island, near Bergen, Norway. The network includes 63 fractures, all with different length. The porous medium spatial dimensions are $700 \text{ m} \times 600 \text{ m}$ with uniform matrix permeability $K_m = \mathbf{I} \text{ m}^2$. All the fractures have the same scalar tangential and normal permeability $K_n = K_f = 10^5 \mathbf{I} \text{ m}^2$ and aperture $\varepsilon = 10^{-2} \text{ m}$. The permeability tensors K_n and K_f are considered to be the effective values, meaning that we incorporate the aperture scaling with ε within the permeability values due to the reduced fracture modeling. See [8, 12] for the detailed description of the scalings. The pressure boundary conditions are imposed on all boundaries, with a linear unitary pressure drop from the left to the right boundary. Throughout all the tests, we use a fixed mesh grid with a typical mesh size $h = 18.75$

m and total of 44765 degrees of freedom. See Figure 4 for an illustration of the domain, the mesh and the numerical solution of this problem.

This more realistic case of a fracture network is chosen to demonstrate the robustness of our auxiliary preconditioners, even with a larger number of fractures in the system and a complex fracture network configuration. Large-scale simulations often require handling those features of fractured porous media, as they often appear in geological rock formations in the subsurface and can significantly influence the stability of the any given solving method. In this case, the sharp tips and very acute intersections of fractures may decrease the shape regularity of the mesh, but also increase the condition number of the system and the number of unknowns, as seen in this example and Figure 4. Therefore, we aim to show that our preconditioners still show a good performance under these challenging conditions.

| α | \mathcal{M}_D | \mathcal{M}_L | \mathcal{M}_U |
|----------|-----------------|-----------------|-----------------|
| 10^2 | 40 (13) | 78 (10) | 79 (9) |
| 10^3 | 15 (9) | 24 (9) | 25 (8) |
| 10^4 | 8 (5) | 10 (5) | 11 (5) |
| 10^5 | 5 (4) | 8 (5) | 4 (5) |
| 10^6 | 6 (28) | 7 (11) | 12 (4) |

Table 4: Performance of the outer FGMRES solver using preconditioners \mathcal{M}_D , \mathcal{M}_L and \mathcal{M}_U in Section 7.2 with regards to varying the scaling parameter α . For each preconditioner, we report number of outer (average inner) iterations needed to reach the prescribed tolerance. The permeability tensors are set to $K_m = \mathbf{I}$, $K_n = K_f = 10^5 \mathbf{I}$ and the mesh size is set to $h = 18.75$.

We first consider different values of the parameter α , with results given in Table 4. As before, the performance of the diagonal \mathcal{M}_D and triangular preconditioners \mathcal{M}_L and \mathcal{M}_U improves with larger values of α , reaching relatively optimal value at $\alpha = 10^5$ for all three preconditioners. This is different from the previous example in Section 7.1 where the best results are given when $\alpha = \max\{1, 100\mathfrak{K}_{min}^{-1}\}$, considering that in this case we have $\mathfrak{K}_{min}^{-1} = 10^{-5}$. However, there are many differences in the problem settings of these two examples that need to be taken into consideration. First, according to Theorem 5.1, the performance of the mixed-dimensional auxiliary space preconditioners can depend on the mixed-dimensional domain Ω and the regularity of the corresponding mesh. In comparison to the example in Section 7.1, the ambient domain in this example is two-dimensional, the domain is more rectangular-type and, due to the complex fracture network configuration, the mesh is less regular. Therefore, we expect a different behavior of both the outer FGMRES and inner GMRES solver in this example. Particularly, this can be seen in Table 4, where the number of outer and inner iterations reduces for larger values of the scaling parameter α , though it started with a large number of iterations in all preconditioners for $\alpha = 10^2$, and for $\alpha = 10^6$ it get slightly larger again. We remind that although larger values of parameter α should improve the performance of the block preconditioners, the divergence part of the inner product (6.14) now dominates, which makes it harder for the inner solver to convergence because of the problem becomes more nearly singular [21, 28].

It is not only the case that the fracture network is more complex, we also have many more fractures included in the domain. This factor should not affect the performance of the preconditioners, which we aim to show in the next set of numerical tests. In the following, we only test the block diagonal preconditioner \mathcal{M}_D since it shows overall best behavior in comparison to the block triangular ones, this particularly evident from Table 4. We also set the scaling parameter $\alpha = 10^5$.

We consider different numbers of fractures included in the original fracture network of 63 fractures in Figure 4. To this end, we randomly select and gradually add more fractures to the network, starting from 1 fracture, to 5, 10, 20, 40 and ultimately all 63 fractures included. We repeat the process four times, creating four different cases, each having either 1, 5, 10, 20 or 40 fractures. See Figure 5 for an illustration of pressure solutions to all four cases, each with 20 randomly selected fractures. The reason to constructing four cases is to eliminate bias in selecting fractures in specific order. We report in Table 5, for all four cases, the number of degrees of freedom N_{dof} and the number of outer (average inner) iterations N_{it} of the FGMRES (GMRES) method preconditioned with the diagonal preconditioner \mathcal{M}_D . It is clear that the preconditioned outer

| N_{fracs} | \mathcal{M}_D | | | | | | | |
|-------------|-----------------|----------|-----------|----------|-----------|----------|-----------|----------|
| | Case 1 | | Case 2 | | Case 3 | | Case 4 | |
| | N_{dof} | N_{it} | N_{dof} | N_{it} | N_{dof} | N_{it} | N_{dof} | N_{it} |
| 1 | 8241 | 6 (3) | 8101 | 7 (2) | 8891 | 6 (3) | 8561 | 7 (3) |
| 5 | 17661 | 7 (3) | 10838 | 6 (3) | 9300 | 6 (3) | 11751 | 6 (3) |
| 10 | 15809 | 6 (3) | 14437 | 7 (3) | 9180 | 6 (3) | 11998 | 6 (3) |
| 20 | 23083 | 7 (3) | 19147 | 6 (4) | 13659 | 7 (3) | 17341 | 6 (4) |
| 40 | 31295 | 5 (4) | 25980 | 6 (4) | 29032 | 7 (4) | 27654 | 6 (4) |
| 63 | 44765 | 5 (4) | 44765 | 5 (4) | 44765 | 5 (4) | 44765 | 5 (4) |

Table 5: Performance of the outer FGMRES solver using preconditioners \mathcal{M}_D , \mathcal{M}_L and \mathcal{M}_U in Section 7.2 with regards to varying number of fractures N_{fracs} in the fracture network. For each preconditioner, we report number of outer (average inner) iterations N_{it} needed to reach the prescribed tolerance. The permeability tensors are set to $K_m = \mathbf{I}$, $K_n = K_f = 10^5 \mathbf{I}$, the mesh size is set to $h = 18.75$ and the scaling parameter $\alpha = 10^5$.

iterative method does not depend on the number of fractures in the fracture network, in all the cases. The same can be seen in the inner solver showing a relatively even number of iterations. Therefore, the robustness of the preconditioner \mathcal{M}_D with regards to the number of fractures in the fracture network is shown, which is consistent with the analysis in the previous sections.

8 Conclusion

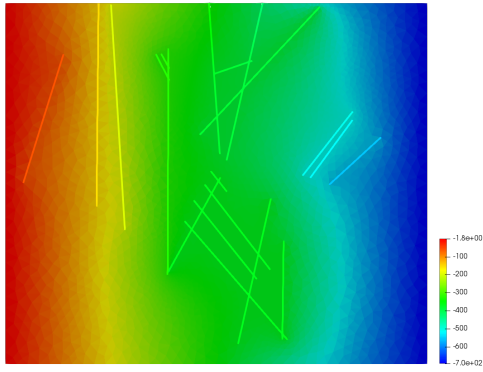
In this work, we have derived nodal auxiliary space preconditioners for discretizations of mixed-dimensional partial differential equations. In order to do so, we have extended the stable regular decomposition, both in continuous and discrete setting, to mixed-dimensional geometries. The resulting decomposition differs from the fixed-dimensional case in the way that we do not consider directly the regular inverse, but we establish the regular decomposition hierarchically by combining the regular decompositions on each sub-manifold of the mixed-dimensional domain. Based on this and the auxiliary space preconditioning framework, we propose robust preconditioners to solving mixed-dimensional elliptic problems. We demonstrate how these preconditioners are derived and implemented with an example of mixed-dimensional model of flow in fractured porous media. The robustness of the preconditioners is also verified of two benchmark numerical experiments of fractured porous media. From the numerical experiments, we also see the need of a robust method for solving Laplacian problem in the mixed-dimensional setting in order to further improve the robustness and effectiveness of the proposed preconditioners. This is the topic for our future work.

9 Acknowledgments

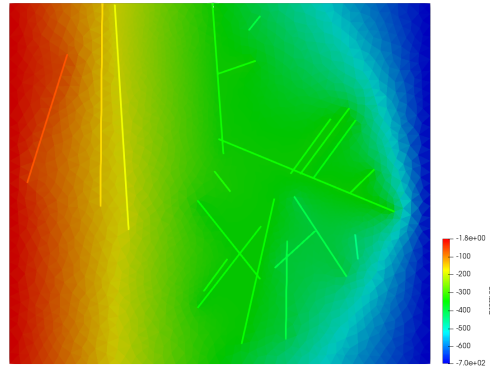
The first author acknowledges the financial support from the TheMSES project funded by Norwegian Research Council grant 250223. The second author thanks the Deutsche Forschungsgemeinschaft (DFG, German Research Foundation) for supporting this work by funding SFB 1313, Project Number 327154368. The work of the third author is partially supported by the National Science Foundation under grant DMS-1620063. A special thanks is extended to Jan M. Nordbotten for valuable comments and discussions on the presented work.

References

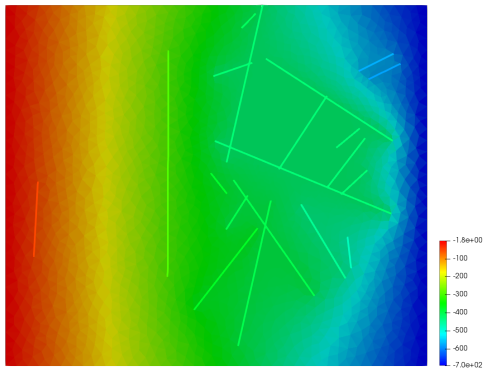
- [1] J. H. ADLER, F. J. GASPAR, X. HU, P. OHM, C. RODRIGO, AND L. T. ZIKATANOV, *Robust preconditioners for a new stabilized discretization of the poroelastic equations*, arXiv:1905.10353 [math.NA], (2019).
- [2] J. H. ADLER, F. J. GASPAR, X. HU, C. RODRIGO, AND L. T. ZIKATANOV, *Robust block preconditioners for biot's model*, in Domain Decomposition Methods in Science and Engineer-



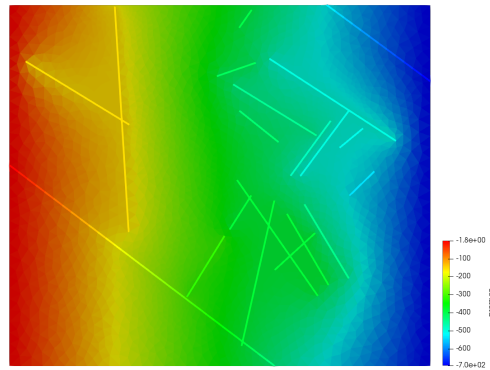
(a) Case 1



(b) Case 2



(c) Case 3



(d) Case 4

Figure 5: Graphical representation of the pressure solution in Example 7.2 with only 20 fractures included. Each Case 1–4 corresponds to selecting randomly 20 fractures from the original set of 63 fractures, without changing the original positioning of the selected fractures within the domain.

ing XXIV, P. E. Bjørstad, S. C. Brenner, L. Halpern, H. H. Kim, R. Kornhuber, T. Rahman, and O. B. Widlund, eds., Cham, 2018, Springer International Publishing, pp. 3–16.

- [3] J. H. ADLER, X. HU, AND L. T. ZIKATANOV, *HAZMATH: A simple finite element, graph and solver library*.
- [4] D. N. ARNOLD, R. S. FALK, AND R. WINTHER, *Finite element exterior calculus, homological techniques, and applications*, Acta numerica, 15 (2006), pp. 1–155.
- [5] J. BEAR, *Hydraulics of groundwater*, Courier Corporation, 2012.
- [6] I. BERRE, W. BOON, B. FLEMISCH, A. FUMAGALLI, D. GLÄSER, E. KEILEGAVLEN, A. SCOTTI, I. STEFANSSON, AND A. TATOMIR, *Call for participation: Verification benchmarks for single-phase flow in three-dimensional fractured porous media*, arXiv preprint arXiv:1809.06926, (2018).
- [7] W. M. BOON, J. M. NORDBOTTEN, AND J. E. VATNE, *Functional analysis and exterior calculus on mixed-dimensional geometries*, tech. rep., arXiv:1710.00556v3 [math.AP], 2018.
- [8] W. M. BOON, J. M. NORDBOTTEN, AND I. YOTOV, *Robust discretization of flow in fractured porous media*, SIAM J. Numer. Anal., 56 (2018), pp. 2203–2233.
- [9] A. BUDIŠA AND X. HU, *Block preconditioners for mixed-dimensional discretization of flow in fractured porous media*, arXiv preprint arXiv:1905.13513, (2019).
- [10] P. G. CIARLET, *Mathematical Elasticity: Volume II: Theory of Plates*, vol. 27, Elsevier, 1997.
- [11] R. FALK AND R. WINTHER, *Local bounded cochain projections*, Mathematics of Computation, 83 (2014), pp. 2631–2656.
- [12] B. FLEMISCH, I. BERRE, W. BOON, A. FUMAGALLI, N. SCHWENCK, A. SCOTTI, I. STEFANSSON, AND A. TATOMIR, *Benchmarks for single-phase flow in fractured porous media*, Advances in Water Resources, 111 (2018), pp. 239–258.
- [13] M. FORTIN AND R. GLOWINSKI, *Augmented Lagrangian Methods: Applications to the Numerical Solution of Boundary-Value Problems*, vol. 15 of Studies in Mathematics and Its Applications, Elsevier, 2000.
- [14] R. HIPTMAIR, *Finite elements in computational electromagnetism*, Acta Numerica, 11 (2002), pp. 237–339.
- [15] R. HIPTMAIR AND C. PECHSTEIN, *Regular decompositions of vector fields – continuous, discrete and structure-preserving*, SAM Research Report No. 2019-18, (2019).
- [16] R. HIPTMAIR AND J. XU, *Nodal auxiliary space preconditioning in $H(\text{curl})$ and $H(\text{div})$ spaces*, SIAM Journal on Numerical Analysis, 45 (2007), pp. 2483–2509.
- [17] X. HU, S. WU, X.-H. WU, J. XU, C.-S. ZHANG, S. ZHANG, AND L. ZIKATANOV, *Combined preconditioning with applications in reservoir simulation*, Multiscale Modeling & Simulation, 11 (2013), pp. 507–521.
- [18] E. KEILEGAVLEN, R. BERGE, A. FUMAGALLI, M. STARNONI, I. STEFANSSON, J. VARELA, AND I. BERRE, *Porepy: An open-source software for simulation of multiphysics processes in fractured porous media*, arXiv:1908.09869 [math.NA], (2019).
- [19] T. V. KOLEV AND P. S. VASSILEVSKI, *Parallel auxiliary space AMG for $H(\text{curl})$ problems*, Journal of Computational Mathematics, 27 (2009), pp. 604–623.
- [20] T. V. KOLEV AND P. S. VASSILEVSKI, *Parallel Auxiliary Space AMG Solver for $H(\text{div})$ Problems*, SIAM Journal on Scientific Computing, 34 (2012), pp. A3079–A3098.

- [21] Y.-J. LEE, J. WU, J. XU, AND L. T. ZIKATANOV, *Robust subspace correction methods for nearly singular systems*, Mathematical Models and Methods in Applied Sciences, 17 (2007), pp. 1937–1963.
- [22] D. LOGHIN AND A. J. WATHEN, *Analysis of preconditioners for saddle-point problems*, SIAM J. Sci. Comput., 25 (2004), pp. 2029–2049.
- [23] K.-A. MARDAL AND R. WINTHER, *Preconditioning discretizations of systems of partial differential equations*, Numer. Linear Algebra Appl., 18 (2011), pp. 1–40.
- [24] S. NEPOMNYASCHIKH, *Decomposition and fictitious domains methods for elliptic boundary value problems*, in Fifth International Symposium on Domain Decomposition Methods for Partial Differential Equations, Philadelphia, PA: Society for Industrial and Applied Mathematics, 1992, pp. 62–72.
- [25] J. M. NORDBOTTEN AND W. M. BOON, *Modeling, structure and discretization of hierarchical mixed-dimensional partial differential equations*, in Domain Decomposition Methods in Science and Engineering XXIV, P. E. Bjørstad, S. C. Brenner, L. Halpern, H. H. Kim, R. Kornhuber, T. Rahman, and O. B. Widlund, eds., Springer International Publishing, 2018, pp. 87–101.
- [26] J. M. NORDBOTTEN AND M. A. CELIA, *Geological storage of CO₂: modeling approaches for large-scale simulation*, John Wiley & Sons, 2011.
- [27] M. SPIVAK, *Calculus on manifolds: a modern approach to classical theorems of advanced calculus*, CRC Press, 2018.
- [28] R. S. TUMINARO, J. XU, AND Y. ZHU, *Auxiliary space preconditioners for mixed finite element methods*, in Domain Decomposition Methods in Science and Engineering XVIII, M. Bercovier, M. J. Gander, R. Kornhuber, and O. Widlund, eds., Berlin, Heidelberg, 2009, Springer Berlin Heidelberg, pp. 99–109.
- [29] J. XU, *The auxiliary space method and optimal multigrid preconditioning techniques for unstructured grids*, Computing, 56 (1996), pp. 215–235.